

ACTIVE: Towards Highly Transferable 3D Physical Camouflage for Universal and Robust Vehicle Evasion

Naufal Suryanto^{1,‡}, Yongsu Kim^{1,2,‡}, Harashta Tatimma Larasati¹, Hyoeun Kang^{1,2}, Thi-Thu-Huong Le¹,
Yoonyoung Hong¹, Hunmin Yang³, Se-Yoon Oh³, Howon Kim^{1,2,*}

¹Pusan National University, South Korea; ²SmartM2M, South Korea; ³Agency for Defense Development (ADD), South Korea

<https://islab-ai.github.io/active-iccv2023/>

Abstract

Adversarial camouflage has garnered attention for its ability to attack object detectors from any viewpoint by covering the entire object’s surface. However, universality and robustness in existing methods often fall short as the transferability aspect is often overlooked, thus restricting their application only to a specific target with limited performance. To address these challenges, we present Adversarial Camouflage for Transferable and Intensive Vehicle Evasion (ACTIVE), a state-of-the-art physical camouflage attack framework designed to generate universal and robust adversarial camouflage capable of concealing any 3D vehicle from detectors. Our framework incorporates innovative techniques to enhance universality and robustness, including a refined texture rendering that enables common texture application to different vehicles without being constrained to a specific texture map, a novel stealth loss that renders the vehicle undetectable, and a smooth and camouflage loss to enhance the naturalness of the adversarial camouflage. Our extensive experiments on 15 different models show that ACTIVE consistently outperforms existing works on various public detectors, including the latest YOLOv7. Notably, our universality evaluations reveal promising transferability to other vehicle classes, tasks (segmentation models), and the real world, not just other vehicles.

1. Introduction

Deep neural networks (DNNs) have achieved tremendous outcomes in a wide range of research fields, especially in computer vision, such as facial recognition and self-driving cars [8, 36, 7]. Despite their remarkable performance, DNNs, including object detection models, are vulnerable to adversarial attacks [2]. Generally, adversarial attacks can be classified into digital attacks and physical attacks [38]. Digital attacks are primarily carried out by

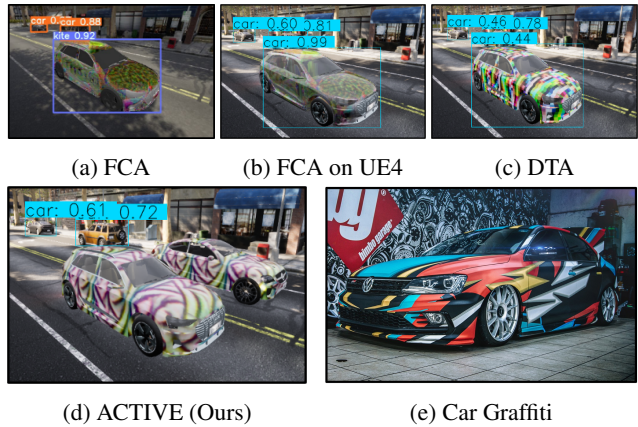


Figure 1: Current state-of-the-art adversarial camouflage, Full-coverage Camouflage Attack (FCA) [37]; (a) is undetected as car in their original result, but (b) is normally detected when fully transferred to Unreal Engine 4 (UE4). (c) The result of the Differentiable Transformation Attack (DTA) [32], with stronger result than FCA, but limited to unnatural mosaic pattern. (d) The result of ACTIVE, which has better attack performance (i.e., not detected as a car at all), is universal (i.e., implementable to other car), and has a natural pattern comparable to (e) a real-world graffiti.

adding small perturbations to pixels of input images. However, digital attacks have limitations in real-world scenarios because they have to manipulate the digital systems that may be configured with security schemes. To alleviate these limitations, physical attacks have been proposed that modify the object in the physical space rather than in the digital.

Nonetheless, physical attacks are more challenging due to the inherently complex physical constraints (camera pose, lighting, occlusion, etc.). Therefore, most physical attack methods exclude the perturbation constraint (i.e., the result can be suspicious). There are mainly two types of methods in physical attacks: adversarial patch and adversarial camouflage. The former [6, 34] is the method of physical

[‡] Equal contribution * Corresponding author

attack by attaching a small, localized patch to an object. It only covers the planar part of the object’s surface and can fail to attack the detector depending on the viewing angles.

Adversarial camouflage methods [47, 43, 41, 37, 32] have been proposed to overcome the limitations of the adversarial patch. This approach covers the whole surface of the object by manipulating the texture of the object, which leads to better attack performance regardless of the viewing angles. Most of these methods use *vehicles* as the target objects due to their crucial role in real-world applications, such as surveillance systems and autonomous driving.

Due to the non-planarity of 3D vehicles, it is more challenging to generate optimal adversarial camouflage than in its 2D counterpart. Since the general 3D rendering is non-differentiable, early research [47, 43] employed a black-box approach to generating adversarial camouflage, inevitably yielding a lower attack performance than the white-box one. More recent research (e.g., DAS [41], FCA [37], and DTA [32]) utilize a neural renderer to acquire the advantage of the white-box approach, which offers differentiability. In particular, DTA proposes its own neural renderer capable of expressing various physical and realistic characteristics. Additionally, it employs its so-called Repeated Texture Projection function to apply the same attack texture to other vehicle types, thus improving universality. However, DTA relies on a simple texture projection, which may result in an inaccurate texture for non-planar shapes. For improving the accuracy and robustness of adversarial camouflage methods, it would be essential to bring forth a more sophisticated texture mapping approach.

In this paper, we propose *Adversarial Camouflage for Transferable and Intensive Vehicle Evasion* (ACTIVE), a state-of-the-art adversarial camouflage framework that greatly enhances robustness, universality, and naturalness compared to previous methods, as shown in Fig. 1. Our contributions can be summarized as follows:

- We utilize *Triplanar Mapping*, a sophisticated texture mapping approach available through the neural renderer, to generate adversarial textures with improved robustness and universality. To the best of our knowledge, the use of this method in generating adversarial camouflage has never been found in literature.
- We employ *Stealth Loss*, our novel attack loss function that minimizes the detection score from all valid classes, resulting in the target vehicle being not only misclassified but also undetectable.
- We improve the naturalness of the adversarial camouflage by utilizing larger texture resolutions than previous works [47, 43, 32] and applying a smooth loss. Furthermore, we introduce a *Camouflage Loss* that can enhance the camouflage of the vehicle against the background.

- Our extensive experiments demonstrate that ACTIVE consistently outperforms previous works, exhibiting improved universality from multiple perspectives: instance-agnostic (available on various vehicle types), class-agnostic (even across different classes such as truck and bus), model-agnostic (performing on various vehicle detectors), task-agnostic (performing on segmentation models), and domain-agnostic (performing in real-world scenarios).

2. Related Works

The Expectation over Transformation (EoT) [4] has emerged as a leading approach in generating robust adversarial examples under various transformations, including variations in viewing distance, angle, and lighting conditions. Consequently, many adversarial camouflage methods [47, 43, 41, 37, 32] incorporate EoT-based algorithms to enhance their attack robustness in the physical scenarios.

Regarding the texture rendering process, differentiability is crucial to enable white-box attacks to obtain optimal adversarial camouflage, whereas non-differentiability of general texture rendering led to the initial proposal of the black-box approach. Zhang et al. [47] proposed CAMOU, utilizing the clone network that imitates the texture rendering and detection process, while Wu et al. [43] suggested finding optimal adversarial texture based on genetic algorithm.

Huang et al. [18] proposed the Universal Physical Camouflage Attack (UPC) as an alternative method for crafting universal adversarial camouflage, which differs from existing black-box approaches. To make UPC effective for non-rigid or non-planar objects, they introduced a set of transformations that can mimic deformable properties. However, subsequent studies [41, 37, 32] have found that the transferability of UPC is limited when it comes to various viewing angles, other models, and different environments due to its inherent limitations of the patch-based method.

More recent research used a neural renderer, which provides a differentiable texture rendering, to improve attack performance. Wang et al. [41] proposed the Dual Attention Suppression (DAS) attack, which suppresses both model and human attention. Meanwhile, Wang et al. [37] proposed the Full-coverage Camouflage Attack (FCA), which is more robust under complex views.

However, Suryanto et al. [32] pointed out that the DAS and FCA used a legacy renderer, which could not reflect various real-world characteristics and complex scenes, such as shadows and light reflections. They proposed the Differentiable Transformation Attack (DTA) that uses their own neural renderer, which provides rendering similar to a photo-realistic renderer. Despite its success, DTA also comes with several limitations. Notably, the method relies on a simple texture projection, which can lead to inaccurate texture mapping. Furthermore, the generated camouflage

features a colorful mosaic pattern, which appears unnatural to human observers. Tab. 1 compares how well existing approaches stack up against the suggested method under various criteria. As shown, our proposal satisfies and achieves all good values under each condition setting compared to prior methods.

Table 1: Comparison of proposed and existing physical camouflage attack methods.

Attack	3D	WB	FC	(1) U	(2) A	(3) N	(4) D	(5) P
AP [6]	×	✓	×	★★	★★	-	★★	-
UPC [18]	×	✓	×	★★	★★	★★	★★	*
CM [47]	✓	×	✓	*	★★	-	-	★★
ER [43]	✓	×	✓	*	★★	-	-	★★
DAS [41]	✓	✓	×	-	*	★★	-	*
FCA [37]	✓	✓	✓	-	*	*	-	*
DTA [32]	✓	✓	✓	*	★★	-	*	★★
Ours	✓	✓	✓	★★	★★	★★	★★	★★

Notes:

3D | White Box (WB) | Full Covering (FC)

(1) Universality (U): * Might be universal, but only optimized on a single instance |

★★ Universal, the adversarial is optimized on multiple instances on the same category

(2) Applicability (A): * Require exact position to place the adversarial |

★★ Can be placed anywhere which satisfies on the target object

(3) Naturalness (N): * Consider naturalness such as using smooth texture |

★★ Have a more constrained setting

(4) Digital Transformation (D): * Affine transformation only |

★★ Both affine transformation and brightness, contrast

(5) Physical Transformation (P): * Camera position only |

★★ Both camera position and physical phenomena

3. Methodology

3.1. Problem Definition

Assume f is a neural renderer that generates optimal adversarial camouflage through white-box attacks based on differentiable rendering. f learns texture rendering by solving Eq. 1,

$$f(x_{ref}, \eta) = x_{ren} \quad (1)$$

where x_{ref} refers to the reference image, which includes the target vehicle, η is the texture variable, and x_{ren} is the rendered image with η . Previously, existing works have utilized neural renderer to generate adversarial camouflage by minimizing the loss function as shown in Eq. 2,

$$\arg \min_{\eta_{adv}} L(h(f(x_{ref}, \eta_{adv})), y) \quad (2)$$

where h is the hypothesis function for the vehicle detector, y is the corresponding detection label output, and $L(h(x), y)$ is the loss function that represents the confidence score of h regarding class y . Thus, solving Eq. 2 involves generating η_{adv} to attack h by minimizing its confidence score.

We have noticed that there are rooms for improvement in at least two aspects. First, most of the neural renderers employed in existing adversarial camouflage methods use

object-dependent texture mapping, such as UV mapping. Therefore, if the vehicle type changes, the previously generated η_{adv} cannot be used. Second, most existing methods only minimize the target class confidence score for y . While this may cause misclassification as a different class than y , the object detection itself may remain. Meanwhile, our proposal employs a method that applies an advanced and object-independent texture mapping approach (i.e., triplanar mapping), which later proves to solve the universality issues. Furthermore, to address both limitations, we introduce Eq. 3,

$$\arg \min_{\eta_{adv}} \mathbb{E}_{v \in V, y \in Y} L(h(f(x_v, \eta_{adv})), y) \quad (3)$$

where V denotes the available vehicle types while Y signifies the available classes of the detector. Solving Eq. 3 aims to: (1) improve universality by generating an attack pattern that is applicable to various vehicles simultaneously, and (2) enhance robustness by minimizing confidence scores for all valid classes to avoid detection as objects themselves.

3.2. ACTIVE Framework

To generate universal and robust adversarial camouflage, we propose the ACTIVE framework, which employs an object-independent texture mapping with a neural renderer and a new attack loss function to cause the vehicle undetectable. The overall framework is as illustrated in Fig. 2.

Triplanar Mapping (TPM). We introduce the use of *triplanar mapping* [26], a texture mapping technique that applies textures to objects by projecting them from three directions using their surface coordinate and surface normal that can be extracted from the depth image. We find this method particularly beneficial for generating object-independent adversarial textures since it does not rely on object-specific texture maps. Thus, we can optimize a common adversarial camouflage for multiple vehicles, making our attack instance-agnostic. Further, we introduce the Neural Texture Renderer (NTR), our improvement of DTN method by Suryanto et al. [32], which works well with our triplanar mapping while effectively preserving various physical characteristics. To our knowledge, we are the first to refine triplanar-mapped texture as the input to the neural renderer for enabling adversarial texture optimization across 3D instances. Our NTR enhances the efficiency of DTN by removing unnecessary elements of DTN, which the detail can be found in the Supplementary Material.

Stealth Loss. We propose *stealth loss*, a novel attack loss function for improving robustness. It considers two representative scores used in object detection models: the class confidence score and the objectness score. First, we minimize the objectness score, which determines the presence of an object in the detector, such as in YOLO families. Moreover, instead of minimizing the maximum confidence

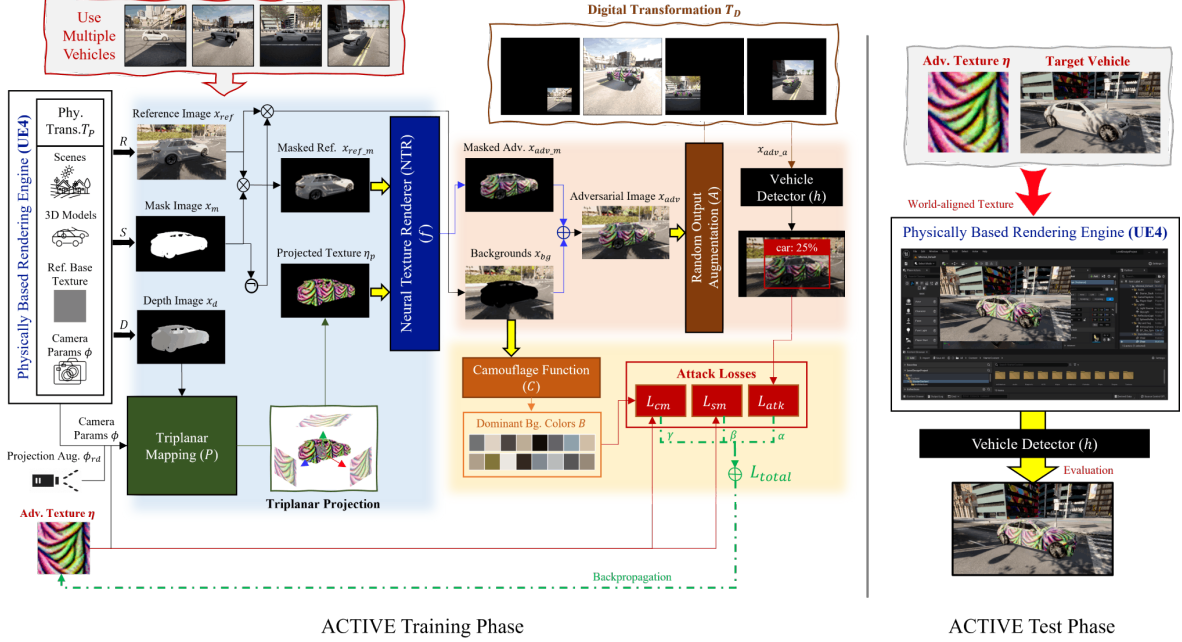


Figure 2: ACTIVE framework for generating universal and robust adversarial camouflage.

score for a specific class, we minimize the maximum confidence score across all classes, making our attack class-agnostic. This approach does not only mislead the model to misclassification, but also considers the possibility of the box being empty of objects. The attack loss L_{atk} is written as Eq. 4,

$$h_d(x) = \begin{cases} h_c(x) \times h_o(x), & \text{if } IoU(h_b(x), gt) > t \\ 0, & \text{otherwise} \end{cases} \quad (4)$$

$$L_{atk}(x) = f_{log}(\max(h_d(x)))$$

where x is an input image of a vehicle detector h , $h_c(x)$ is the confidence score of h for x , $h_o(x)$ is the objectness score of h for x , $h_b(x)$ is the detection result of h for x in the form of the bounding box, $IoU(h_b(x), gt)$ is the Intersection over Union (IoU) between the bounding box $h_b(x)$ and the ground-truth, gt , and t is a custom IoU threshold. We define $h_d(x)$ as a detection score, which is the product of the confidence score and the objectness score. $f_{log}(n) = -\log(1 - n)$ is a log loss when the ground truth is zero. Then, minimizing L_{atk} has the effect of minimizing both the confidence and objectness scores. Note that we only assign a value to the detection score for valid boxes with IoU greater than t , otherwise set it as zero. Thereby, the valid detection performance of the object detection model can be effectively lowered because the loss is applied only to the box that detects the object closely, and otherwise is excluded.

Random Output Augmentation (ROA). We propose an *ROA module* to enhance the texture robustness by various digital transformations [4]. Specifically, the module

takes the output of the NTR, i.e., the adversarial example, and further augments it by applying random transformations such as scaling, translation, brightness, and contrast. While the NTR already provides robustness against *various physical* transformations, ROA allows for attaining an additional level of robustness with *digital* transformations to simulate changes happening in the real world to a certain extent, which to the best of our knowledge, have not been considered in most adversarial camouflage methods.

Smooth Loss. We utilize a smooth loss (i.e., Total Variation (TV) loss [24]) to improve the smoothness of the generated camouflage, which we define as L_{sm} in Eq. 5,

$$L_{sm}(\eta) = \frac{1}{N_{sm}} \sum_{i,j} f_{log}(|\eta_{i,j} - \eta_{i+1,j}|) + f_{log}(|\eta_{i,j} - \eta_{i,j+1}|) \quad (5)$$

where $\eta_{i,j}$ is a pixel in a texture, η , at coordinate (i, j) and $N_{sm} = (H-1) \cdot (W-1)$ is a scale factor with texture image height, H , and texture image width, W . We slightly modify the loss for scale adjustment and normalization compared to the original TV loss. That is, L_{sm} is low when the values of adjacent pixels are close to each other. Thus, minimizing L_{sm} improve the smoothness of the adversarial camouflage.

Camouflage Loss. We propose a camouflage loss to improve camouflage for human vision as well as computer vision. There are several ways to computationally measure camouflage effectiveness, the most common method being to measure the target-background similarity [35]. We use a method to extract the most dominant background colors and force the object texture color to be similar. First, we employ a camouflage function based on K-means clustering to ex-

tract the most dominant colors from all background images [45, 19, 44]. Next, we utilize Non-Printability Score (NPS) loss [30] to regulate the object texture color set. While it was originally proposed to craft a color set that is comprised mostly of colors reproducible by the printer, we replace the printable color set used in the original NPS loss with the most dominant background color set. The camouflage loss, L_{cm} , can be expressed as Eq. 6,

$$L_{cm}(\eta, B) = \frac{1}{N_{cm}} \sum_{i,j} f_{log}(\min_{b \in B} |b - \eta_{i,j}|) \quad (6)$$

where $N_{cm} = H \cdot W$ is a scale factor of camouflage loss, and B is the most dominant background color set. We can acquire the adversarial camouflage, which has a similar color to the background, by minimizing L_{cm} . Finally, our total loss, L_{total} , is constructed as Eq. 7,

$$L_{total} = \alpha L_{atk} + \beta L_{sm} + \gamma L_{cm} \quad (7)$$

where α , β , and γ are the weights to control the contribution of each loss function. The full pipeline of the ACTIVE framework for generating adversarial camouflage by minimizing L_{total} is illustrated in Fig. 2 and Alg. 1.

Algorithm 1 ACTIVE adversarial camouflage generation

Input: Physical transformation set T_P , Digital transformation set T_D , Rendering function R , Segmentation function S , Depth function D , Triplanar mapping P , NTR f , ROA module A ,

Output: Adversarial camouflage η

(1) Export x_{ref} , x_m , x_d , x_{ref-m} , and x_{bg} from the rendering engine

$$x_{ref} \leftarrow R(T_P), x_m \leftarrow S(T_P), x_d \leftarrow D(T_P)$$

$$x_{ref-m} \leftarrow x_{ref} \times x_m, x_{bg} \leftarrow x_{ref} \times \neg x_m$$

(2) Export B by Camouflage function C

$$B \leftarrow C(x_{bg})$$

(3) Generate adversarial camouflage η

Initialize η with random values

for number of training iterations **do**

Select the minibatch sample from x_{ref-m}, x_m, x_{bg}

Derive ϕ, ϕ_{rd} corresponding to each x_{ref-m} from T_P

$$\eta_p \leftarrow P(\eta, x_d, \phi + \phi_{rd})$$

$$x_{adv-m} \leftarrow f(x_{ref-m}, \eta_p)$$

$$x_{adv} \leftarrow x_{adv-m} + x_{bg}$$

$$x_{adv-a} \leftarrow A(x_{adv}, T_D)$$

Calculate $L_{atk}(x_{adv-a}), L_{sm}(\eta), L_{cm}(\eta, B)$ by Eq. 4, 5, 6

Set L_{total} by Eq. 7

Update η for minimizing L_{total} via backpropagation

end for

4. Experiments

We perform comprehensive experiments to investigate the performance of our proposed method on multiple aspects, including robustness and universality. Each experiment and its comparison with previous works are designed with specific criteria. However, due to limited space, we only present the essential information and leave the detail to the Supplementary Materials.

4.1. Implementation Details

Environment and Datasets. We implement our attacking framework using TensorFlow 2 [1] and utilize CARLA [12] on Unreal Engine 4 (UE4) [13] as a physically-based simulator for training and evaluation, following [32]. We synthesize our own dataset for training and evaluation with various photo-realistic settings. We select five types of cars on CARLA for attack texture generation and robustness evaluation, and another different five for universality evaluation, where they are excluded from texture optimization. For NTR model training, a total of 50,625 and 150,000 photo-realistic images are used for training and testing, respectively. Regarding attack pattern generation, another 15,000 images for reference are employed. As for attack evaluation, we render the generated attack pattern on multiple cars using world-aligned texture in Unreal Engine to produce a repeated pattern while ignoring the texture UV Map, with 14,400 images for a single texture evaluation.

NTR. We build an NTR with four encoder-decoder layers using DenseNet architecture [16] (following [32]) and train using 20 epochs. Our experiment verifies that the network trained with only nine selected colors are able to generalize 50 random colors on the test, achieving 0.985 SSIM (comparable to 0.986 SSIM in the original DTN setting), but with 82% less data. Details in Supplementary Material.

Attack Parameters. Our attack texture is optimized using Adam [21] with 30 epochs. For ROA, we use 0.25 random brightness, [0.75, 1.5] random contrast, and [0.25, 1.0] random scale. For projection augmentation on triplanar mapping, we use [-0.5, 0.5] random shift and [-0.25, 0.25] random scale. For loss hyperparameters, we use $\alpha = 1.0$ with IoU threshold $t = 0.5$, $\beta = 0.25$, and $\gamma = 0.25$ as default. Also, we set the base texture resolution to 64×64 .

4.2. Robustness Evaluations

From Digital to Physical Simulation. First, we perform a comparative experiment to investigate the effectiveness of existing rendering methods, including ours, by evaluating the performance of attack textures in the original pipeline compared to physical simulation (UE4). For a fair comparison with prior works, we follow DAS [41] and FCA [37] by selecting the same simulated town and Audi E-Tron car in CARLA, then optimizing the textures targeting YOLOv3

Table 2: Digital-to-physical simulation comparison. Values are Average Precision@0.5 (%) of car in YOLOv3.

Methods	Orig. Rendering	Adv. Exm.	Phy. Sim.
Normal	UE4	-	99.57
DAS [41]	+ NMR	88.55	96.09
FCA [37]	+ NMR	52.05	92.28
DTA [32]	+ RTP & DTN	16.91	41.95
Ours	+ TPM & NTR	1.28	7.29



Figure 3: Rendering comparison of white-box 3D adv. camouflage methods: Adv. example from original pipeline vs. Fully transferred to physical simulation (UE4). Zoom in.

[27]. In detail, DAS and FCA utilize Neural Mesh Renderer (NMR) [20] to optimize the 3D car texture and attach it to the simulated town as background, while DTA [32] utilizes Repeated Texture Projection (RTP) and DTN to simply project repeated texture and render it to the reference image. Meanwhile, ours utilizes TPM and NTR for more accurate repeated texture mapping and rendering.

As shown in Tab. 2 and Fig. 3, adversarial example produced by our optimization pipeline results in a very high attack performance compared to related works, even after fully transferred to physical simulation. DAS exhibits poor performance due to its partial texture coverage which is aligned with [37, 32]. FCA can successfully evade the detection in the original pipeline but is fully detected in the physical simulation with a high score. We observe DAS and FCA textures are mostly obscured by light reflections, which cannot be represented by their rendering method. DTA, which considers physical transformations but inaccurate texture mapping, causes misdetection in the original pipeline but is still detected in the physical simulation with a low score. In contrast, ours can successfully evade detection almost perfectly, thanks to our accurate texture mapping.

Attack Comparison on Physically-Based Simulation.

We run a more extensive attack comparison by using diverse camera poses and evaluated models. Specifically, we follow FCA to evaluate all methods on SSD [23], Faster R-CNN (FrRCNN) [28], and Mask R-CNN (MkRCNN) [15] as the black-box model while keeping YOLOv3 as the target.

The attack comparison results are depicted in Tab. 3, from which we can infer that our method consistently has the best attack performance on all models, both on a single-

Table 3: Attack comparison on physically-based simulation. Values are Average Precision@0.5 (%) of car.

Methods	Single-Stage Detector		Two-Stage Detector	
	YOLOv3	SSD	FrRCNN	MkRCNN
Normal	90.67	92.20	87.84	94.30
Random	70.01	79.01	74.41	69.09
Naive Cam.	60.26	59.48	58.71	67.21
DAS [41]	88.53	84.28	84.31	88.48
FCA [37]	76.92	76.35	74.09	80.27
CAMOU [47]	59.20	68.02	67.84	62.31
ER [43]	58.02	70.77	62.45	61.30
DTA [32]	33.33	47.80	47.44	49.85
Ours	19.52	33.56	41.70	45.08

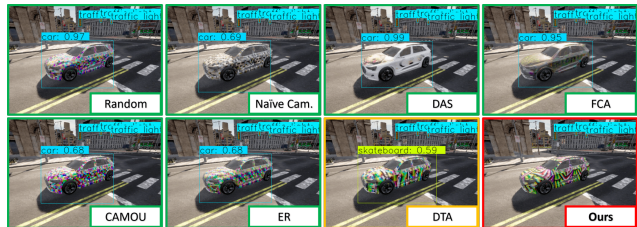


Figure 4: Attack comparison samples. Zoom for detail.

stage and two-stage detector. Note that we include a random and naive camouflage pattern to show the model’s robustness against arbitrary textures. Again, we can see that DAS and FCA, whose limitation prevents them from considering physical parameters during optimization, yield much lower performance. Also, while CAMOU [47] and ER [43] consider physical parameters from the simulator during optimization, such black-box attacks do not guarantee an optimum result. On the other hand, DTA [32] yields much better results since it accounts for both physical parameters and white-box attacks. Nevertheless, it consistently underperforms compared to ours.

We also provide the model prediction sample of the compared methods in Fig. 4, showing the model can still correctly predict Random, DAS, and FCA textured cars with high detection scores. FCA failure illustrates the importance of considering physical parameters, as the car’s metallic material may cause light reflections that can hide the texture. Naive, CAMOU, and ER decrease the detection score, but still insufficiently to result in misclassification. Alternatively, DTA texture *does* misclassify the object, but nowhere near our method, which renders the car undetected.

Fig. 5 shows the summarized performance of each camera pose; values are car AP@0.5, averaged from all evaluated models. It visualizes how our method invariably outperforms previous works on all viewing conditions. As implied, our method is relatively stable under various distances compared to other methods. Additionally, we observe that varied camera pitches have a greater impact on attack performance than other poses.

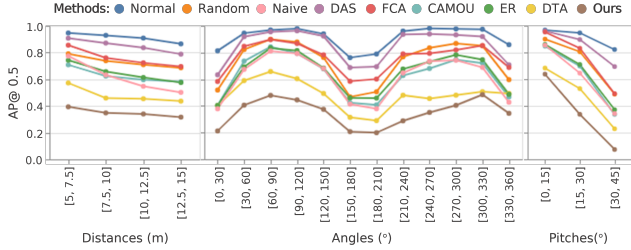


Figure 5: Attack comparison on different camera poses. Values are AP@0.5 of the car averaged from all models.

Table 4: Universality evaluation where target objects, models, and scenes differ from the training. AP@0.5 (%) of car.

Methods	Single-Stage		Two-Stage		Transformer	
	YLv3	YLv7	DRCN	SRCN	DDTR	PVT
Normal	85.98	92.54	83.20	82.55	83.83	88.59
Random	66.93	85.65	69.59	70.43	47.77	78.42
Naive Cam.	60.73	69.62	55.68	64.08	49.91	67.45
UPC [18]	83.48	90.00	80.58	78.36	73.64	86.61
CAMOU [47]	60.19	82.67	63.78	62.93	33.33	68.77
ER [43]	58.90	82.18	62.06	62.54	37.34	73.96
DTA [32]	32.24	59.39	45.72	43.68	19.43	56.05
Ours	22.55	41.55	30.38	42.00	14.69	51.54

4.3. Universality Evaluations

Transferability Comparison on Different Settings.

For this experiment, we use various brand-new models, including YOLOv7 (YLv7) [36], Dynamic R-CNN (DRCN) [46], Sparse R-CNN (SRCN) [31], Deformable DETR (DDTR) [48], and Pyramid Vision Transformer (PVT) [42] to evaluate transferability over diverse modern architectures. All models are considered black-box except for YOLOv3 [27], used for texture generation in the previous section. The results of car AP@0.5 are presented in Tab. 4, showing that our method has the best performance on all models. It is interesting to see that YOLOv7 is so robust that Random, UPC [18], CAMOU, and ER can only slightly reduce the car AP@0.5. Nevertheless, even in the black-box setting, our method can significantly reduce the YOLOv7 performance. More surprisingly, our attack method is robust even in the case of the Transformer-based vision models, although they are generally known to be more resilient to adversarial attacks than CNNs and have low transferability from CNNs [25, 5, 3]. Considering most studies claiming their robustness only conduct digital attack experiments, it is a discovery that transformer-based model can be vulnerable to physical attacks such as our adversarial camouflage. This indicates our method is also *model-agnostic*.

Fig. 6 displays the sample prediction results of YOLOv7 on evaluated methods. The model can correctly predict naive camouflage, UPC, CAMOU, and ER textured cars, but with consistently higher detection scores compared to previous evaluations. One of the DTA-textured cars results



Figure 6: Transferability to different settings. Zoom in.

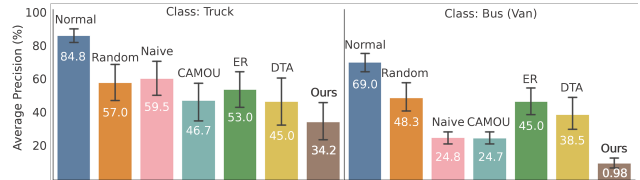


Figure 7: Transferability to different class (Truck and Bus).

in misclassification, but the other is still detected correctly with a fairly low detection score. It is different from ours, which consistently makes the cars undetected, further verifying the universality of our method as *instance-agnostic*.

Transferability Comparison on Different Class. We evaluate the textures when applied to different classes (i.e., truck and bus), use all evaluated models in the last experiment, and group the result in Fig. 7. As shown, our method constantly outperforms others, demonstrating that ACTIVE is *class-agnostic*, thanks to our stealth loss that considers all instead of specific class labels during optimization.

Transferability Comparison on Different Task. We further evaluate all methods' universality by testing the generated texture on a publicly available pretrained segmentation model: MaX-DeepLab-L [39] and Axial-DeepLab [40] with SWideRNet [10] Backbone. We test on both Cityscape [11] and COCO [22] pretrained models, and exclude high-pitch cameras because the Cityscape dataset only uses low-pitch data. Furthermore, we only evaluate the pixel accuracy (%) of the car label to show how the texture can downgrade the prediction of the target object. Again, the experiment result in Tab. 5 shows that our method significantly outperforms the previous works. Additionally, Fig. 8 visualizes the sample of how our method makes the car invisible from the segmentation model (either predicted as road or ignored), while other methods correctly predict as car, which also confirms our method produces *task-agnostic* texture.

Transferability to Real World. Following [32], we conduct a real-world evaluation by constructing two 1:10-scaled Tesla Model 3s with a 3D printer and wrapping the texture onto the body of the car: one for a normal and another for our camouflaged car targeting YOLOv3. Fig. 9 shows the normal car model is well detected, whereas the adversarial camouflaged car model is not detected as a car at all. Furthermore, we also evaluate practical real-time ob-

Table 5: Universality evaluation on a different task (i.e., Segmentation Model). Values are pixel accuracy (%) of car.

Methods	Cityscape Pretrained		COCO Pretrained
	MaX-DL-L	Axl-DL-SW	MaX-DL-L
Normal	90.70	92.76	89.77
Random	78.20	88.24	81.68
Naive Cam.	50.23	74.78	64.11
UPC [18]	74.70	83.66	75.85
CAMOU [47]	62.12	71.66	64.18
ER [43]	71.55	85.70	71.17
DTA [32]	31.53	55.68	32.85
Ours	17.45	32.04	23.46

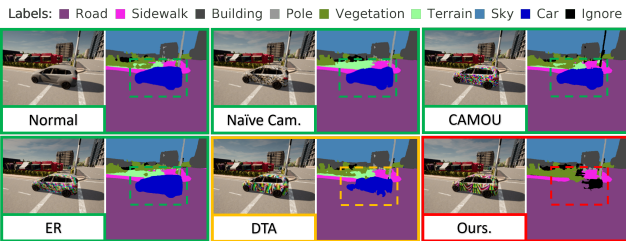


Figure 8: Transferability to segmentation model. Zoom in.



Figure 9: Real-world evaluation using two scaled cars. The upper row is the normal car model, while the bottom row is the adversarial camouflaged car model. Zoom for detail.

Table 6: AP@0.5 (%) of target car in real-world evaluation.

Methods	Real-time Object Detector				
	YLv3	MbNetv2	EfDetD2	YLX-L	YLv7
Normal	90.83	80.83	96.25	96.25	95.00
Ours	8.75	26.27	26.25	40.41	48.75

ject detectors widely used in the real world to show that our method transfers to the real-world (i.e., *domain-agnostic*): MobileNetV2 (MbNetv2) [29], EfficientDet-D2 (EfDetD2) [33], YOLOX-L (YLX-L) [14], YOLOv7 (YLv7) [36], and also the target model, YOLOv3 (YLv3), shown in Tab. 6.

4.4. Ablation Study

Impact of Proposal on Performance and Naturalness.

We evaluated our proposed components, including modules and losses, using ablation studies with default parameters. We used DTA [32] as a baseline since our approach has a similar pipeline. The results in Table 7 demonstrate that each of our proposed components plays a crucial role in enhancing the attack performance. Specifically, utilizing both

Table 7: Ablation study for each proposed module and loss.

Proposed Losses (YLv3 - Car AP@.5)	Proposed Modules (Normal Car: 93.01)				
	Raw	w/ TPM	w/ ROA	Full	Avg. (Std.)
L_{atk} (DTA [32])	60.48	48.21	48.43	24.66	45±15
L_{atk} (Stealth Loss)	60.13	43.70	38.85	22.48	41±15
$L_{atk} + L_{sm}$	58.90	43.36	36.00	20.21	39±16
$L_{atk} + L_{cm}$	56.17	42.04	38.66	24.34	40±13
$L_{atk} + L_{sm} + L_{cm}$	57.81	50.87	40.70	28.22	44±13
Avg. (Std.)	59±2	46±4	41±5	24±3	

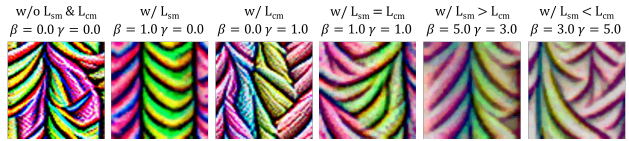


Figure 10: Visual textures comparison with different losses.

TPM and ROA modules significantly impacts performance enhancement, with an average improvement of 35%.

Although our proposed losses have a lesser impact on performance, they play an important role in texture naturalness, leading to trade-offs between the two. As illustrated in Fig. 10, omitting L_{sm} outputs a rough texture, whereas excluding L_{cm} makes it more colorful and bright. Employing the stealth loss with only smooth loss yields the best performance, downgrading the car AP@0.5 to 20.21%. More details are available in Supplementary Materials.

5. Discussions

Societal Implications. Adversarial camouflage poses harmful repercussions for self-driving cars since there exists a highly feasible attack scenario, e.g., legally painting cars with adversarial texture [47, 32]. Enhancements in robustness and universality by ACTIVE can amplify the danger as existing public detectors are still highly vulnerable, signifying the importance of research in model robustness.

Limitation. Even though ACTIVE produces a more natural pattern similar to graffiti, the texture is still abstract.

6. Conclusion

We have presented ACTIVE, a physical camouflage attack framework for 3D objects for enhanced universality and robustness. Verified in our comprehensive evaluations, ACTIVE surpasses the performance of existing works—and notably, demonstrates its capability as a model, instance, class, task, and domain-agnostic framework.

Acknowledgments. This work was supported by the Agency For Defense Development Grant Funded by the Korean Government (UE221150WD), and by the MSIT (Ministry of Science and ICT), Korea, under the Convergence security core talent training business (Pusan National University) support program (IITP-2023-2022-0-01201) supervised by the IITP (Institute for Information & Communications Technology Planning & Evaluation).

References

- [1] Martín Abadi, Ashish Agarwal, Paul Barham, Eugene Brevdo, Zhifeng Chen, Craig Citro, Greg S. Corrado, Andy Davis, Jeffrey Dean, Matthieu Devin, Sanjay Ghemawat, Ian Goodfellow, Andrew Harp, Geoffrey Irving, Michael Isard, Yangqing Jia, Rafal Jozefowicz, Lukasz Kaiser, Manjunath Kudlur, Josh Levenberg, Dandelion Mané, Rajat Monga, Sherry Moore, Derek Murray, Chris Olah, Mike Schuster, Jonathon Shlens, Benoit Steiner, Ilya Sutskever, Kunal Talwar, Paul Tucker, Vincent Vanhoucke, Vijay Vasudevan, Fernanda Viégas, Oriol Vinyals, Pete Warden, Martin Wattenberg, Martin Wicke, Yuan Yu, and Xiaoqiang Zheng. TensorFlow: Large-scale machine learning on heterogeneous systems, 2015. Software available from tensorflow.org. **5**
- [2] Naveed Akhtar and Ajmal Mian. Threat of adversarial attacks on deep learning in computer vision: A survey. *IEEE Access*, 6:14410–14430, 2018. **1**
- [3] Ahmed Aldahdooh, Wassim Hamidouche, and Olivier Deforges. Reveal of vision transformers robustness against adversarial attacks. *arXiv preprint arXiv:2106.03734*, 2021. **7**
- [4] Anish Athalye, Logan Engstrom, Andrew Ilyas, and Kevin Kwok. Synthesizing robust adversarial examples. In *International conference on machine learning*, pages 284–293. PMLR, 2018. **2, 4**
- [5] Philipp Benz, Soomin Ham, Chaoning Zhang, Adil Karjauv, and In So Kweon. Adversarial robustness comparison of vision transformer and mlp-mixer to cnns. *arXiv preprint arXiv:2110.02797*, 2021. **7**
- [6] Tom B. Brown, Dandelion Mané, Aurko Roy, Martín Abadi, and Justin Gilmer. Adversarial patch. *CoRR*, abs/1712.09665, 2017. **1, 3**
- [7] Nicolas Carion, Francisco Massa, Gabriel Synnaeve, Nicolas Usunier, Alexander Kirillov, and Sergey Zagoruyko. End-to-end object detection with transformers. In *European conference on computer vision*, pages 213–229. Springer, 2020. **1**
- [8] Junyi Chai, Hao Zeng, Anming Li, and Eric W.T. Ngai. Deep learning in computer vision: A critical review of emerging techniques and application scenarios. *Machine Learning with Applications*, 6:100134, 2021. **1**
- [9] Kai Chen, Jiaqi Wang, Jiangmiao Pang, Yuhang Cao, Yu Xiong, Xiaoxiao Li, Shuyang Sun, Wansen Feng, Ziwei Liu, Jiarui Xu, Zheng Zhang, Dazhi Cheng, Chenchen Zhu, Tianheng Cheng, Qijie Zhao, Buyu Li, Xin Lu, Rui Zhu, Yue Wu, Jifeng Dai, Jingdong Wang, Jianping Shi, Wanli Ouyang, Chen Change Loy, and Dahua Lin. MMDetection: Open mmlab detection toolbox and benchmark. *arXiv preprint arXiv:1906.07155*, 2019. **14**
- [10] Liang-Chieh Chen, Huiyu Wang, and Siyuan Qiao. Scaling wide residual networks for panoptic segmentation. *arXiv:2011.11675*, 2020. **7, 14**
- [11] Marius Cordts, Mohamed Omran, Sebastian Ramos, Timo Rehfeld, Markus Enzweiler, Rodrigo Benenson, Uwe Franke, Stefan Roth, and Bernt Schiele. The cityscapes dataset for semantic urban scene understanding. In *Proc. of the IEEE Conference on Computer Vision and Pattern Recognition (CVPR)*, 2016. **7, 14**
- [12] Alexey Dosovitskiy, German Ros, Felipe Codevilla, Antonio Lopez, and Vladlen Koltun. CARLA: An open urban driving simulator. In *Proceedings of the 1st Annual Conference on Robot Learning*, pages 1–16, 2017. **5, 11**
- [13] Epic Games. Unreal engine. **5, 13**
- [14] Zheng Ge, Songtao Liu, Feng Wang, Zeming Li, and Jian Sun. Yolox: Exceeding yolo series in 2021. *arXiv preprint arXiv:2107.08430*, 2021. **8, 14, 20**
- [15] Kaiming He, Georgia Gkioxari, Piotr Dollár, and Ross Girshick. Mask r-cnn. In *Proceedings of the IEEE international conference on computer vision*, pages 2961–2969, 2017. **6, 14, 16**
- [16] Gao Huang, Zhuang Liu, Laurens Van Der Maaten, and Kilian Q Weinberger. Densely connected convolutional networks. In *Proceedings of the IEEE conference on computer vision and pattern recognition*, pages 4700–4708, 2017. **5**
- [17] Jonathan Huang, Vivek Rathod, Chen Sun, Menglong Zhu, Anoop Korattikara, Alireza Fathi, Ian Fischer, Zbigniew Wojna, Yang Song, Sergio Guadarrama, et al. Speed/accuracy trade-offs for modern convolutional object detectors. In *Proceedings of the IEEE conference on computer vision and pattern recognition*, pages 7310–7311, 2017. **14**
- [18] Lifeng Huang, Chengying Gao, Yuyin Zhou, Changqing Zou, Cihang Xie, Alan L. Yuille, and Ning Liu. UPC: learning universal physical camouflage attacks on object detectors. In *CVPR*, volume abs/1909.04326, 2019. **2, 3, 7, 8, 13**
- [19] Qi Jia, Ziqiang Lin, Jianghua Hu, Jun Liu, Liyan Zhu, and Junyu Liu. Design and evaluation of facial camouflage pattern. In *Proceedings of the 2019 International Conference on Artificial Intelligence and Computer Science, AICS 2019*, page 818–821, New York, NY, USA, 2019. Association for Computing Machinery. **5**
- [20] Hiroharu Kato, Yoshitaka Ushiku, and Tatsuya Harada. Neural 3d mesh renderer. In *Proceedings of the IEEE conference on computer vision and pattern recognition*, pages 3907–3916, 2018. **6, 13**
- [21] Diederik P Kingma and Jimmy Ba. Adam: A method for stochastic optimization. *arXiv preprint arXiv:1412.6980*, 2014. **5**
- [22] Tsung-Yi Lin, Michael Maire, Serge J. Belongie, Lubomir D. Bourdev, Ross B. Girshick, James Hays, Pietro Perona, Deva Ramanan, Piotr Dollár, and C. Lawrence Zitnick. Microsoft COCO: common objects in context. *CoRR*, abs/1405.0312, 2014. **7, 14**
- [23] Wei Liu, Dragomir Anguelov, Dumitru Erhan, Christian Szegedy, Scott Reed, Cheng-Yang Fu, and Alexander C Berg. Ssd: Single shot multibox detector. In *European conference on computer vision*, pages 21–37. Springer, 2016. **6, 14, 16**
- [24] Aravindh Mahendran and Andrea Vedaldi. Understanding deep image representations by inverting them. In *CVPR*, pages 5188–5196. IEEE Computer Society, 2015. **4, 22**
- [25] Kaleel Mahmood, Rigel Mahmood, and Marten Van Dijk. On the robustness of vision transformers to adversarial examples. In *Proceedings of the IEEE/CVF International Conference on Computer Vision*, pages 7838–7847, 2021. **7**

- [26] Kris Nicholson and Ashish Naicker. Gpu based algorithms for terrain texturing. 2008. [3](#), [11](#), [12](#)
- [27] Joseph Redmon and Ali Farhadi. Yolov3: An incremental improvement. *arXiv preprint arXiv:1804.02767*, 2018. [6](#), [7](#), [13](#), [14](#), [16](#), [17](#), [20](#)
- [28] Shaoqing Ren, Kaiming He, Ross Girshick, and Jian Sun. Faster r-cnn: Towards real-time object detection with region proposal networks. *Advances in neural information processing systems*, 28, 2015. [6](#), [13](#), [14](#), [16](#)
- [29] Mark Sandler, Andrew Howard, Menglong Zhu, Andrey Zhmoginov, and Liang-Chieh Chen. Mobilenetv2: Inverted residuals and linear bottlenecks. In *Proceedings of the IEEE conference on computer vision and pattern recognition*, pages 4510–4520, 2018. [8](#), [14](#), [20](#)
- [30] Mahmood Sharif, Sruti Bhagavatula, Lujio Bauer, and Michael K. Reiter. Accessorize to a crime: Real and stealthy attacks on state-of-the-art face recognition. In *Proceedings of the 2016 ACM SIGSAC Conference on Computer and Communications Security, CCS '16*, page 1528–1540, New York, NY, USA, 2016. Association for Computing Machinery. [5](#)
- [31] Peize Sun, Rufeng Zhang, Yi Jiang, Tao Kong, Chenfeng Xu, Wei Zhan, Masayoshi Tomizuka, Lei Li, Zehuan Yuan, Changhu Wang, et al. Sparse r-cnn: End-to-end object detection with learnable proposals. In *Proceedings of the IEEE/CVF conference on computer vision and pattern recognition*, pages 14454–14463, 2021. [7](#), [14](#), [17](#)
- [32] Naufal Suryanto, Yongsu Kim, Hyoeun Kang, Harashta Tatimma Larasati, Youngyeo Yun, Thi-Thu-Huong Le, Hunmin Yang, Se-Yoon Oh, and Howon Kim. Dta: Physical camouflage attacks using differentiable transformation network. In *Proceedings of the IEEE/CVF Conference on Computer Vision and Pattern Recognition (CVPR)*, pages 15305–15314, June 2022. [1](#), [2](#), [3](#), [5](#), [6](#), [7](#), [8](#), [11](#), [13](#), [14](#)
- [33] Mingxing Tan, Ruoming Pang, and Quoc V Le. Efficientdet: Scalable and efficient object detection. In *Proceedings of the IEEE/CVF conference on computer vision and pattern recognition*, pages 10781–10790, 2020. [8](#), [14](#), [20](#)
- [34] Simen Thys, Wiebe Van Ranst, and Toon Goedemé. Fooling automated surveillance cameras: adversarial patches to attack person detection. *CoRR*, abs/1904.08653, 2019. [1](#)
- [35] Alexander Toet and Maarten A. Hogervorst. Review of camouflage assessment techniques. In Karin U. Stein and Ric Schleijsen, editors, *Target and Background Signatures VI*, volume 11536, page 1153604. International Society for Optics and Photonics, SPIE, 2020. [4](#)
- [36] Chien-Yao Wang, Alexey Bochkovskiy, and Hong-Yuan Mark Liao. Yolov7: Trainable bag-of-freebies sets new state-of-the-art for real-time object detectors. *arXiv preprint arXiv:2207.02696*, 2022. [1](#), [7](#), [8](#), [14](#), [17](#), [20](#)
- [37] Donghua Wang, Tingsong Jiang, Jialiang Sun, Weien Zhou, Zhiqiang Gong, Xiaoya Zhang, Wen Yao, and Xiaoqian Chen. Fca: Learning a 3d full-coverage vehicle camouflage for multi-view physical adversarial attack. In *Proceedings of the AAAI Conference on Artificial Intelligence*, volume 36, pages 2414–2422, 2022. [1](#), [2](#), [3](#), [5](#), [6](#), [13](#)
- [38] Donghua Wang, Wen Yao, Tingsong Jiang, Guijiang Tang, and Xiaoqian Chen. A survey on physical adversarial attack in computer vision, 2022. [1](#)
- [39] Huiyu Wang, Yukun Zhu, Hartwig Adam, Alan Yuille, and Liang-Chieh Chen. Max-deeplab: End-to-end panoptic segmentation with mask transformers. In *Proceedings of the IEEE/CVF conference on computer vision and pattern recognition*, pages 5463–5474, 2021. [7](#), [14](#), [18](#), [19](#)
- [40] Huiyu Wang, Yukun Zhu, Bradley Green, Hartwig Adam, Alan Yuille, and Liang-Chieh Chen. Axial-deeplab: Stand-alone axial-attention for panoptic segmentation. In *European Conference on Computer Vision*, pages 108–126. Springer, 2020. [7](#), [14](#), [18](#), [19](#)
- [41] Jiakai Wang, Aishan Liu, Zixin Yin, Shunchang Liu, Shiyu Tang, and Xianglong Liu. Dual attention suppression attack: Generate adversarial camouflage in physical world. In *2021 IEEE/CVF Conference on Computer Vision and Pattern Recognition (CVPR)*, pages 8561–8570, 2021. [2](#), [3](#), [5](#), [6](#), [13](#)
- [42] Wenhai Wang, Enze Xie, Xiang Li, Deng-Ping Fan, Kaitao Song, Ding Liang, Tong Lu, Ping Luo, and Ling Shao. Pyramid vision transformer: A versatile backbone for dense prediction without convolutions. In *Proceedings of the IEEE/CVF International Conference on Computer Vision*, pages 568–578, 2021. [7](#), [14](#), [17](#)
- [43] Tong Wu, Xuefei Ning, Wenshuo Li, Ranran Huang, Huazhong Yang, and Yu Wang. Physical adversarial attack on vehicle detector in the carla simulator. *CoRR*, abs/2007.16118, 2020. [2](#), [3](#), [6](#), [7](#), [8](#), [13](#)
- [44] Houdi Xiao, Zhipeng Qu, Mingyun Lv, Yi Jiang, Chuanzhi Wang, and Ruiyu Qin. Fast self-adaptive digital camouflage design method based on deep learning. *Applied Sciences*, 10(15), 2020. [5](#)
- [45] Heng Fu Yang and Jian Ping Yin. An adaptive digital camouflage scheme using visual perception and k-mean clustering. In *Research in Materials and Manufacturing Technologies*, volume 834 of *Advanced Materials Research*, pages 1091–1094. Trans Tech Publications Ltd, 1 2014. [5](#)
- [46] Hongkai Zhang, Hong Chang, Bingpeng Ma, Naiyan Wang, and Xilin Chen. Dynamic r-cnn: Towards high quality object detection via dynamic training. In *European conference on computer vision*, pages 260–275. Springer, 2020. [7](#), [14](#), [17](#)
- [47] Yang Zhang, Hassan Foroosh, Philip David, and Boqing Gong. Camou: Learning physical vehicle camouflages to adversarially attack detectors in the wild. In *International Conference on Learning Representations*, 2018. [2](#), [3](#), [6](#), [7](#), [8](#), [13](#)
- [48] Xizhou Zhu, Weijie Su, Lewei Lu, Bin Li, Xiaogang Wang, and Jifeng Dai. Deformable {detr}: Deformable transformers for end-to-end object detection. In *International Conference on Learning Representations*, 2021. [7](#), [14](#), [17](#)

Appendices

Supplementary Material

A. Overview

This supplementary material describes the details of our implementation and evaluation results that can not be included in the main paper due to page limit. Furthermore, additional experiments and more evaluation samples for all experiments on the main paper are also presented.

B. Algorithm Details

B.1. Triplanar Mapping

In this section, we provide a detailed algorithm and figures for triplanar mapping [26]. Algorithm 2 and Figure 11 describe the step-by-step process of extracting a projected texture using triplanar mapping.

Algorithm 2 Triplanar Mapping Algorithm

Input: Depth Image x_d , Camera Parameters ϕ , Projection Augmentation ϕ_{rd} , Adversarial Texture η

Output: Projected Texture η_p

(1) Extract Surface Normal x_{SN} and Surface World Coordinates x_{SWC}

Extract camera intrinsic matrix ϕ_{in} and extrinsic matrix ϕ_{ex} from ϕ

Compute 3D Local Coordinates x_{LC} from ϕ_{in} and x_d

$x_{SWC} \leftarrow x_{LC} \times \phi_{ex}$

Compute x_{SN} from x_{SWC} using the cross product of two tangent vectors

(2) Extract Triplanar Mask

Compute Triplanar Mask x_{TM} based on the highest absolute value of x_{SN} for each axis

Compute x_{TM_x} , x_{TM_y} , x_{TM_z} masked for each axis

(3) Extract Projected Texture η_p

Compute the Repeated Surface Coordinates x_{RSC} by modulating the x_{SWC} with the repeated texture size based on ϕ_{rd}

Take the UV indices of x_{UV_x} , x_{UV_y} , x_{UV_z} from each axis of Repeated Surface Coordinates x_{RSC}

Assign the projected texture η_{p_x} , η_{p_y} , η_{p_z} for each axis from η mapped with x_{UV_x} , x_{UV_y} , x_{UV_z}

$\eta_{p_{x.m}} \leftarrow \eta_{p_x} \times x_{TM_x}$, $\eta_{p_{y.m}} \leftarrow \eta_{p_y} \times x_{TM_y}$, $\eta_{p_{z.m}} \leftarrow \eta_{p_z} \times x_{TM_z}$

$\eta_p \leftarrow \eta_{p_{x.m}} + \eta_{p_{y.m}} + \eta_{p_{z.m}}$

B.2. Framework Procedure

This section describes the optimization of our adversarial texture using the ACTIVE framework. Drawing inspiration from the DTA framework [32], we employ the Neural Texture Renderer (NTR) for rendering our triplanar-mapped textures onto target vehicles while maintaining various physical properties. Prior to optimizing the adversarial texture, it is necessary to train the NTR in advance. A detailed explanation of the NTR can be found in Section D. Subsequently, during the ACTIVE training phase, we generate the optimal adversarial texture by minimizing L_{total} . To further evaluate the attack performance, we conduct a physical simulation (on UE4) wherein our adversarial texture is applied as a world-aligned texture to the target vehicle in UE4, as illustrated in the ACTIVE test phase in Figure 2 of our main paper.

C. Implementation Details

C.1. Dataset

Cars. We select multiple types of cars that are available on the CARLA [12] simulator. Five types of cars used for attack texture generation and robustness evaluation are Audi Etron, Citroen C3, Mercedes-Benz Coupe, Nissan Patrol, and Charger 2020. Additionally, five other cars used for universality evaluation are BMW GrandTourer, Audi A2, Mercedes-Benz C-Class, Jeep Wrangler Rubicon, and Tesla Model 3. All cars are visualized in Fig. 12.

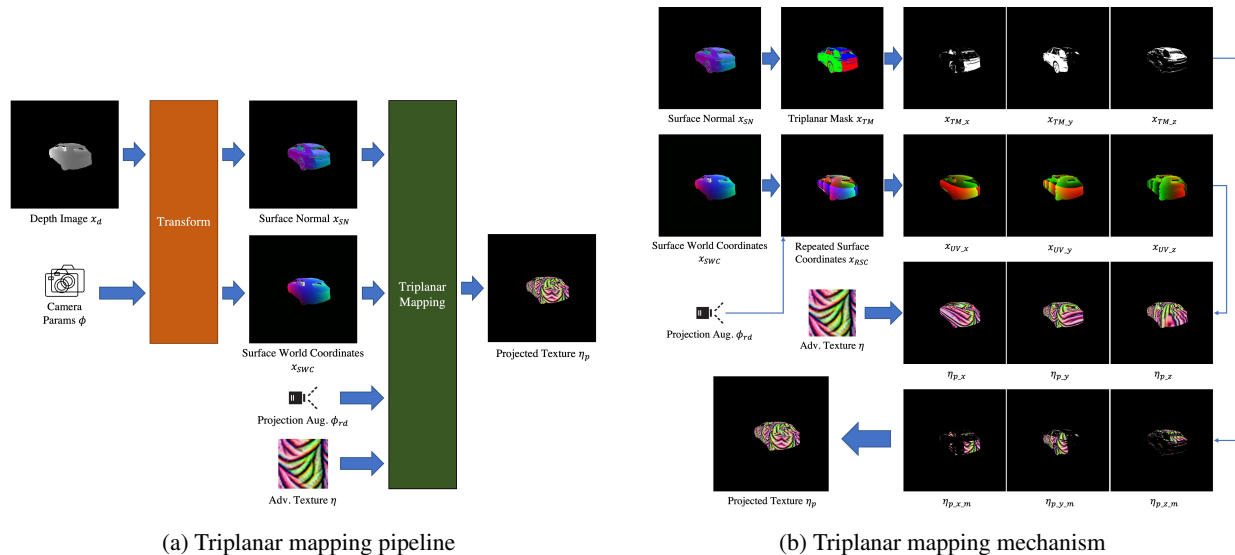


Figure 11: Detailed pipeline and mechanism of Triplanar mapping [26]

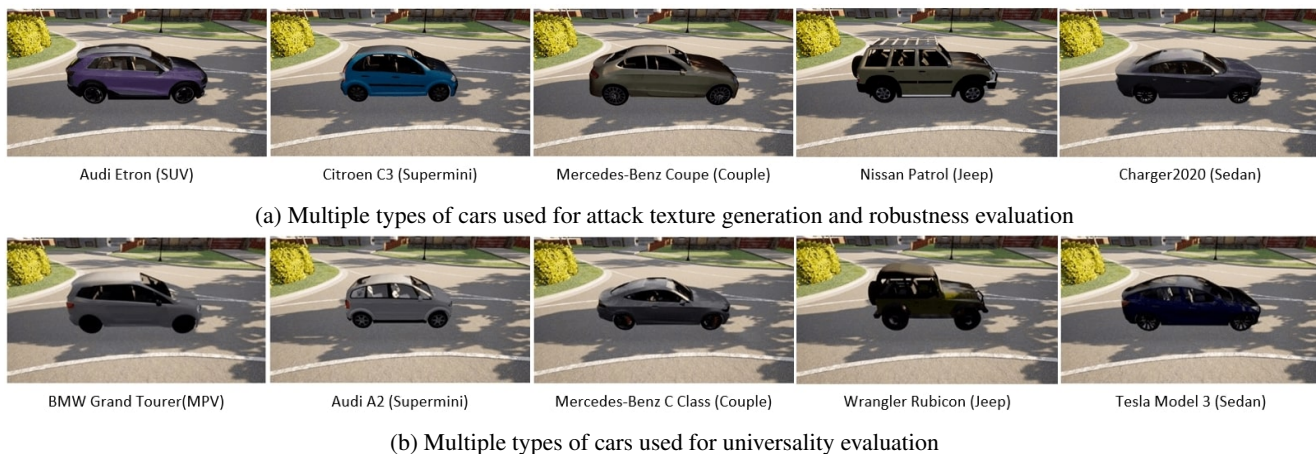


Figure 12: All cars used in our evaluation

For NTR Model Training. We select a map in CARLA and randomly choose 75 random locations for training and 50 different locations for testing. On each location, we generate a car dataset using a camera with a 5-meters distance, 15-degree pitch, and every 30-degree rotation. For each transformation, we gradually change the car types and textures with eight boundary colors and one gray color (as reference image) for training. Additionally, we select 50 random colors for testing. In summary, we employ 50,625 photo-realistic images for training (consisting 5 cars x 75 positions x 12 camera poses x 9 colors), and 150,000 images for testing (consisting 5 cars x 50 positions x 12 camera poses x 50 colors).

For Attack Texture Generation. We use the same cars and camera poses, then choose 250 random locations on the same map to synthesize the reference images. In summary, we use 15,000 photo-realistic images as reference x_{ref} (consisting 5 cars x 250 positions x 12 camera poses x 1 color). For each dataset, we also synthesize the car mask (i.e., the target object).

For Attack Texture Evaluation. For robustness, we evaluate Audi Etron at 50 random locations, while for universality, we assess multiple cars at 20 random locations. We use wider camera transformation to evaluate attacks on untrained camera distributions as default. We also define multiple camera settings, including $[[5, 7.5], [7.5, 10], [10, 12.5], [12.5, 15]]$ meter distances, $[[0, 15], [15, 30], [30, 45]]$ pitch degrees, and $[[0, 30], [30, 60], \dots, [330, 360]]$ rotation degrees. Each value is selected randomly within the range for each evaluation sample. A total of 14,400 images (consisting 5 cars x 20 positions x 4 distances x 3 pitches x 12 angles) for a single texture evaluation are used in our experiments.

C.2. Compared Methods

We provide detailed parameter setup of compared methods: Dual Attention Suppression (DAS) [41], Full-coverage Camouflage Attack (FCA) [37], Universal Physical Camouflage (UPC) [18] CAMOU [47], Enlarge-and-Repeat (ER) [43], and Differentiable Transformation Attack (DTA) [32] in our experiment. Except for texture taken from original codes, we re-optimize all methods targeting YOLOv3 [27] on Audi Etron car, and use the same simulated town for a fair comparison. Additionally, we include random and naive camouflage patterns to evaluate the model’s robustness against arbitrary textures.

DAS and FCA. These methods use Neural Mesh Renderer (NMR) [20] to optimize the adversarial camouflage over a 3D car and attach it to the background, which is CARLA simulated town. We use the original texture from their official codes (DAS: <https://github.com/nlsde-safety-team/DualAttentionAttack>, FCA: <https://github.com/idrl-lab/Full-coverage-camouflage-adversarial-attack>) for our evaluations. Specifically, both textures are optimized for Audi Etron and CARLA Town10. We follow FCA for generating texture targeting YOLOv3 [27] as the white box model. Since these methods depend on a specific 3D UV map, we only evaluate them on robustness evaluation.

UPC. This method outputs a masked patch that can be attached to the target surface. Since UPC has different settings to reproduce in our environments and is specifically designed for targeting Faster R-CNN [28], we execute their official code: <https://github.com/mesunhlf/UPC-tf> and keep the original attack setup on cars, then use their attack patches in our environment. Following [32], we utilize decals in Unreal Engine to apply UPC patches onto target car surfaces, covering the hood, doors, rooftop, and back to ensure visibility from diverse perspectives. Since UPC has a different setting from ours, we only evaluate this method in transferability comparison. Fig. 13 shows samples taken from related works’ original papers (left) and how we fully transfer the texture on Unreal Engine 4 [13] (right).

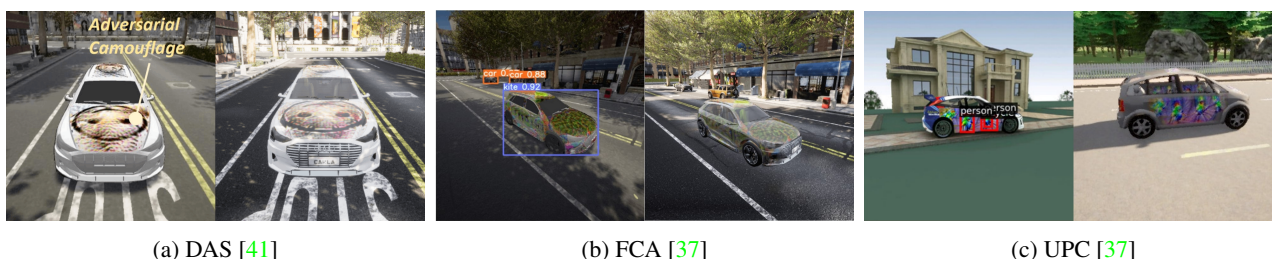


Figure 13: Transferring textures from the original paper (left) to our evaluation setting by fully rendering it on Unreal Engine 4 with epic settings (right).

CAMOU, ER, and DTA. These methods output repeated patterns that cover all target object surfaces as physical camouflage. We choose the same 16×16 texture resolution as the best original setting that forms mosaic-like patterns. We closely replicate the original papers’ approach, but we rebuild the environment and target models same as our evaluation setup (optimizing texture on Audi Etron and targeting YOLOv3 [27]). For CAMOU, we generate the camouflage pattern using the same clone network architecture and other parameters as the original paper. For ER, we use the same parameters as the original paper, except changing the $p = 3$ and $r = 1$ parameters to produce the same 16×16 texture. For DTA, we use NTR as neural renderer in our paper and optimize the texture using the original parameters. All generated textures and the rendered cars are shown in Fig. 14.

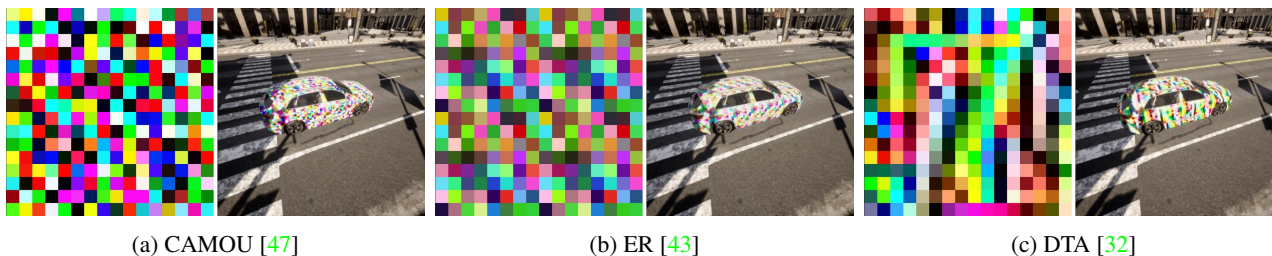


Figure 14: Re-implementation of previous works in our test environment. For each figure, the left side depicts the generated camouflage pattern, while the right side depicts the result of a car rendered by repeated texture using world-aligned texture.

In conclusion, the tables in our main paper were designed with *specific criteria* in mind. In particular, Tab. 2 compares only adversarial camouflage methods based on *Neural Renderer* (i.e., DAS, FCA, and DTA), aimed at assessing its suitability for digital-to-physical transferability. Next, Tab. 3 compares methods that can directly attack the *same target model* (YOLOv3), *vehicle*, and *simulated town*, with Random and Naive camouflage serving as additional benchmarks for robustness against arbitrary texture. Subsequently, UPC was *omitted* in Tab. 3 due to its loss being designed *only for attacking Faster R-CNN*. In contrast, Tabs. 4 and 5 place UPC for comparing universality but *exclude* DAS and FCA due to their *object-dependent textures* cannot be universally applied to different cars.

C.3. Evaluated Models

We evaluate our method on multiple publicly-available state-of-the-art COCO [22] pre-trained object detection models including EfficientDet-D2 [33], YOLOv3 [27], SSD [23], Faster R-CNN [28], Mask R-CNN [15], YOLOv7 [36], Dynamic R-CNN [46], Sparse R-CNN [31], Deformable DETR [48], Pyramid Vision Transformer [42], MobileNetV2 [29], and YOLOX-L [14], with the default score threshold set to 0.30. Furthermore, we also evaluate the attack patterns on state-of-the-art pre-trained panoptic segmentation model including Max-DeepLab-L [39] and Axial-DeepLab [40] with SWideRNet [10] Backbone either pretrained on COCO [22] or Cityscape [11] dataset. For the object detection task, we evaluate the target car AP@0.5, while for the segmentation task, we evaluate the target car pixel accuracy. The details of all evaluated models, including model variant, publication venue, and implementation framework, are available in Table 8 for object detection models and Table 9 for segmentation models.

Table 8: All COCO pre-trained object detection models used in our evaluations. Models are sorted by publication year.

Model Name	Model Variant	Venue	Year	ML Framework	Implementation	Link
Faster R-CNN	ResNet50	NPIS	2015	TensorFlow	TF Object Detection API [17]	Here
SSD	ResNet50-FPN	ECCV	2016	TensorFlow	TF Object Detection API [17]	Here
Mask R-CNN	Inception ResNetV2	ICCV	2017	TensorFlow	TF Object Detection API [17]	Here
YOLOv3	YOLOv3	ArXiv	2018	TensorFlow	TF Re-implementation	Here
MobileNetv2	FPN Lite	CVPR	2018	TensorFlow	TF Object Detection API [17]	Here
EfficientDet	EfficientDet-D2	CVPR	2020	TensorFlow	TF Object Detection API [17]	Here
Dynamic R-CNN	ResNet50	ECCV	2020	Pytorch	MMDetection [9]	Here
Pyramid Vision Transformer	PVT-S	ICCV	2021	Pytorch	MMDetection [9]	Here
Deformable DETR	Two-Stage DDTR	ICLR	2021	Pytorch	MMDetection [9]	Here
Sparse R-CNN	ResNet50-FPN	CVPR	2021	Pytorch	MMDetection [9]	Here
YOLOX	YOLOX-L	ArXiv	2021	TensorFlow	TF Re-implementation	Here
YOLOv7	YOLOv7	ArXiv	2022	Pytorch	Official Implementation	Here

Table 9: All pre-trained panoptic segmentation models used in our evaluations. Models are sorted by publication year.

Model Name	Model Variant	Venue	Year	Pre-trained Dataset	Implementation	Link
Axial-DeepLab	Axial-SWideRNet-(1, 1, 4.5)	ECCV	2020	Cityscape	TF DeepLab2	Here
MaX-DeepLab	MaX-DeepLab-L	CVPR	2021	Cityscape	TF DeepLab2	Here
MaX-DeepLab	MaX-DeepLab-L	CVPR	2021	COCO	TF DeepLab2	Here

D. Neural Texture Renderer (NTR)

D.1. Improvement from Differentiable Transformation Network (DTN)

In this section, we present Neural Texture Renderer (NTR), the improvement of DTN by Suryanto et al. [32]. In particular, we found several redundancies in the DTN, especially in the Transformation Features *TF* and training process. Here, we describe per point how we managed to improve DTN in our NTR.

Redundancy in Transformation Features. DTN as in [32] uses four *TF*, including *TF Subtractor* + ReLU, *TF Adder*, *TF Multiplier*, and *TF Final Adder* that are assumed to cover all basic transformations. We theorize that the first two layers are redundant; the last two are already sufficient for encoding the *TF*. Therefore, we only use *TF Multiplier* and *TF Final Adder* in our final Transformation Features *TF* that are similar to weight and bias in Neural Network design. Our NTR architecture using the dense connection is depicted in Fig. 15a.

Redundancy in Dataset. DTN uses 50 flat random color textures for training the network. We believe this is inefficient, as we want to train the network with multiple objects. We hypothesize that training the network with eight boundary colors in RGB space and gray [128, 128, 128] as the reference color is enough to make the network generalize other colors. The eight boundary colors consist of the primary colors (red [255, 0, 0], green [0, 255, 0], blue [0, 0, 255]), secondary colors (magenta [255, 0, 255], yellow [255, 255, 0], cyan [0, 255, 255]), white [255, 255, 255], and black [0, 0, 0], as in Fig. 15b.

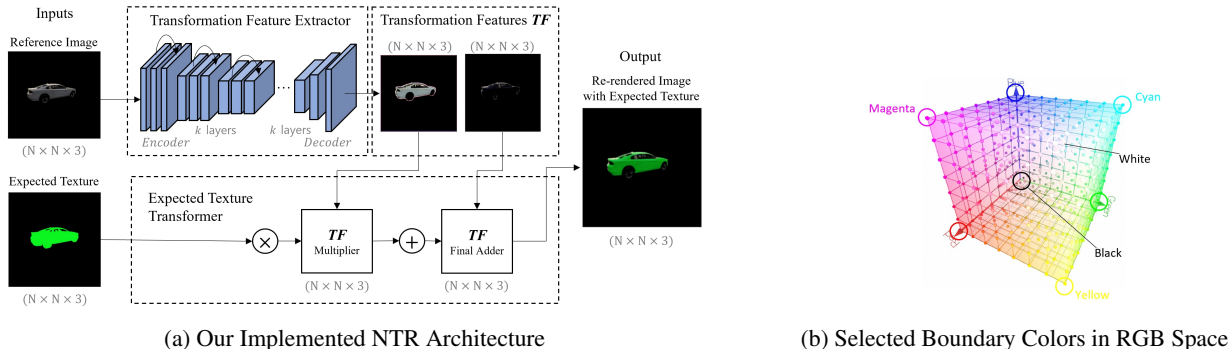


Figure 15: Neural Texture Renderer (NTR) Architecture and Improvement from DTN

D.2. NTR Evaluation

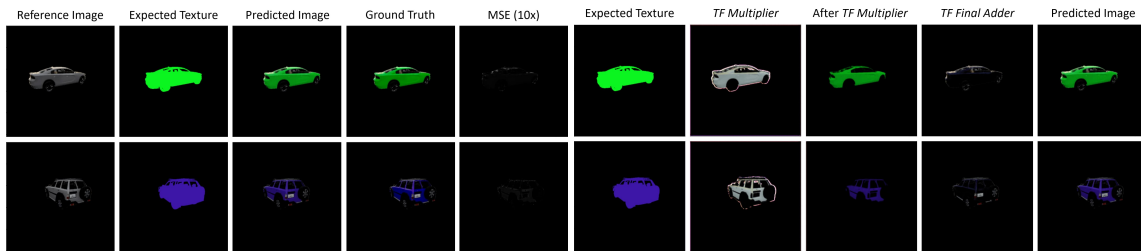
We then perform experiments to evaluate our hypotheses about redundancy in the DTN design. In particular, we train several models using the same machine, and each model is trained with 32 batch sizes for 20 epochs using a single Nvidia Tesla V100 GPU and Intel Xeon E5-2696 CPU. Evaluation results are as shown in Tab. 10, with DTN as the baseline. From the table, we can infer that training the model with only eight boundary colors and gray is enough to enable generalizing the test set, resulting in 82% efficiency. Furthermore, removing redundant TF does not hurt the performance, showing that the last two TF are enough to encode the expected transformation features.

Table 10: NTR Evaluation

Model	N Colors	Total Dataset	Training Time	Tess Loss	Test SSIM
DTN (/w dense connection, k_layers=4)	50	281,250	20.4 hours	0.0312	0.986
+ Trained with Boundary Colors	9	50625	3.7 hours	0.0314	0.985
++ Removed Redundant TF	9	50625	3.7 hours	0.0314	0.985

D.3. NTR Sample Predictions

Here, we present the sample prediction of NTR on the test set after the training is completed. Fig. 16a shows sample prediction result consisting of the reference image containing the target object, expected texture, predicted image (i.e., the output of NTR), ground truth, and MSE (i.e., the error between the predicted image and ground truth). As shown, NTR can learn how to render the expected texture given the reference image. Fig. 16b shows the process of transforming expected texture using the encoded TF. We can observe that TF multiplier is enough to encode the color transformation with the expected texture. TF multiplier can encode how the texture is minimized or emphasized and remove the non-applied texture part. The TF final adder enhances the image from the TF multiplier and adds the non-applied texture part from the reference.



(a) NTR sample predictions on test set (b) Transforming expected texture with the encoded TF

Figure 16: NTR Sample Predictions

E. Robustness Evaluation Details

E.1. Detailed Performance on Various Camera Poses

We evaluate YOLOv3 [27] (a white-box model), and SSD [23], Faster R-CNN [28], Mask R-CNN [15] (which are black-box models) for each distance, rotation, and pitch. As shown in Fig. 17 and 18, our method has better attack performance than other methods and is relatively stable under various camera poses in most cases.

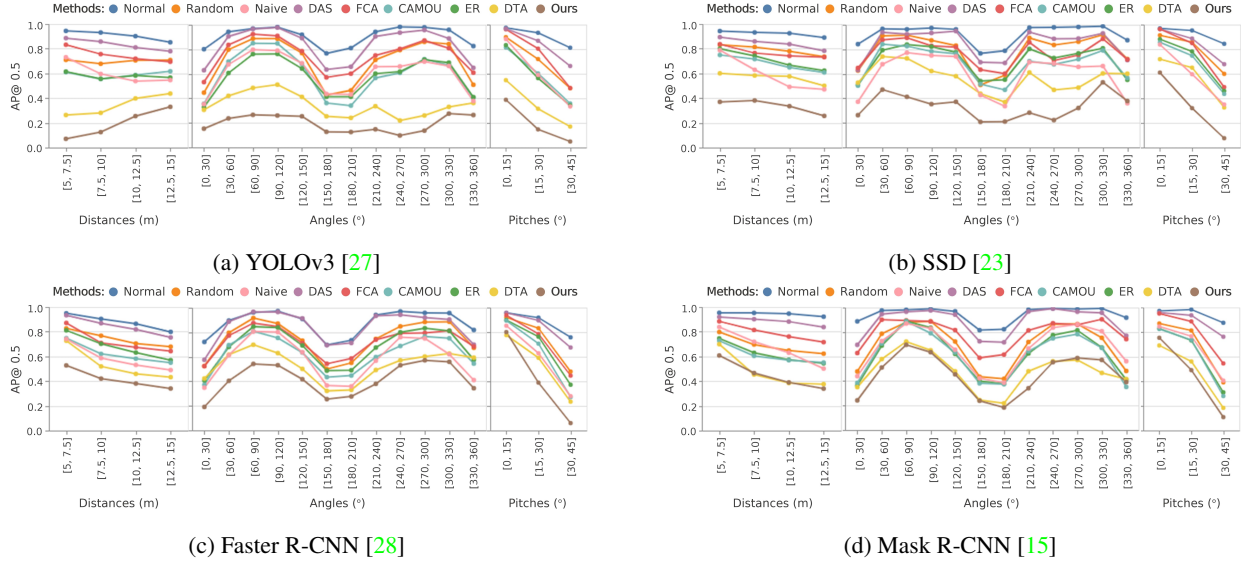


Figure 17: Attack comparison on different camera poses. Values are Average Precision @0.5 of the target car.

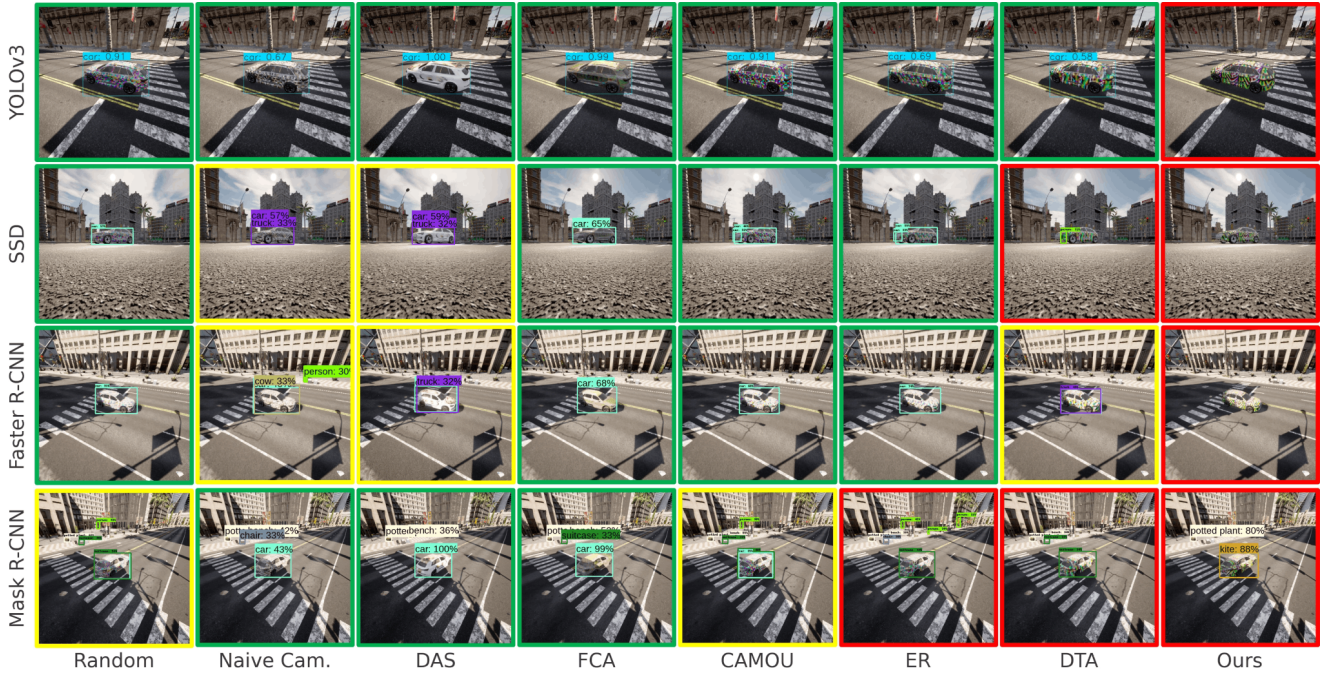


Figure 18: Sample predictions for each method and evaluated model. Green = correct; Yellow = partially correct; Red = misdetection. Zoom for detail.

F. Universality Evaluation Details

We provide the detailed experimental results of the universality evaluation. First, we evaluate the transferability by trying out our method in different settings (i.e., different from the settings used in the robustness evaluation). We also evaluate the transferability on different classes (i.e., truck and bus) and a different task (i.e., segmentation models). Finally, we fabricate the car models with a 3D printer to evaluate our method’s transferability to the real world.

F.1. Transferability to Different Settings

Here, we use different settings from the robustness evaluation: different cars (as in Fig. 12b), different scenes, and diverse modern object detection architecture such as YOLOv7 [36], Dynamic R-CNN [46], Sparse R-CNN [31], Deformable DETR (DDTR) [48], and Pyramid Vision Transformer (PVT) [42]. As shown in Fig. 19, it is observed that our method outperforms previous works in most cases, and even when being evaluated in different settings as a black-box attack. Sample prediction for each model can be seen in Fig. 20.

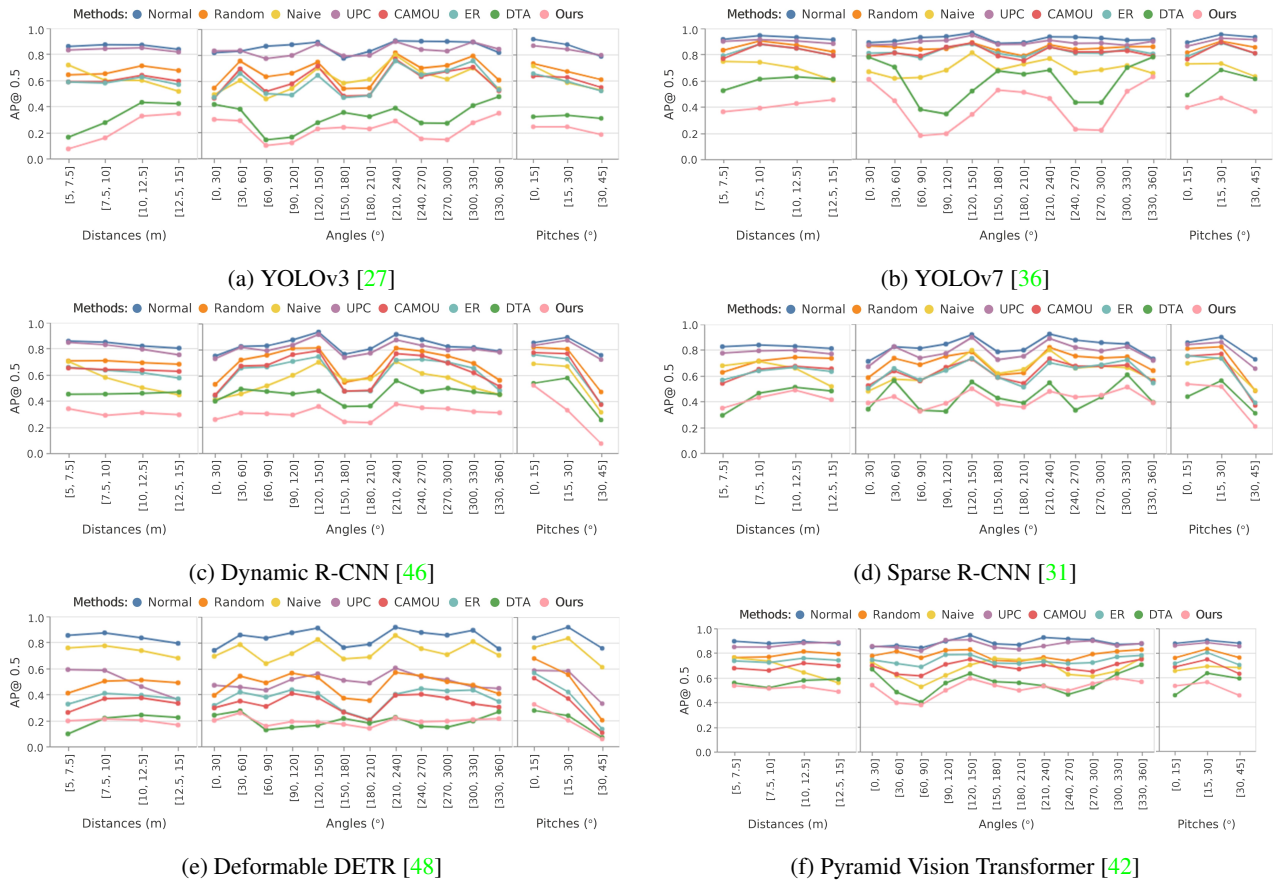
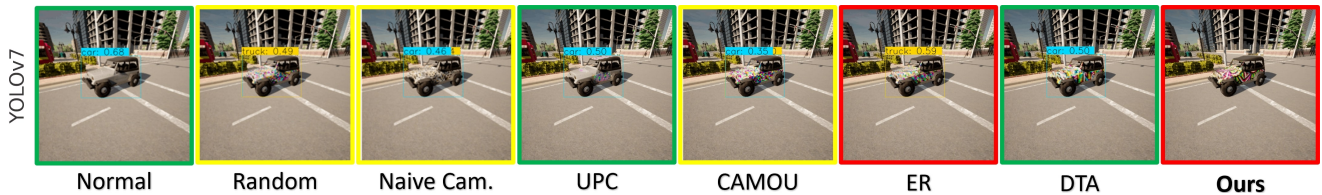


Figure 19: Universality evaluation on different camera poses. Target objects, models, and scenes differ from the training setting. Values are Average Precision @0.5 of the target car.



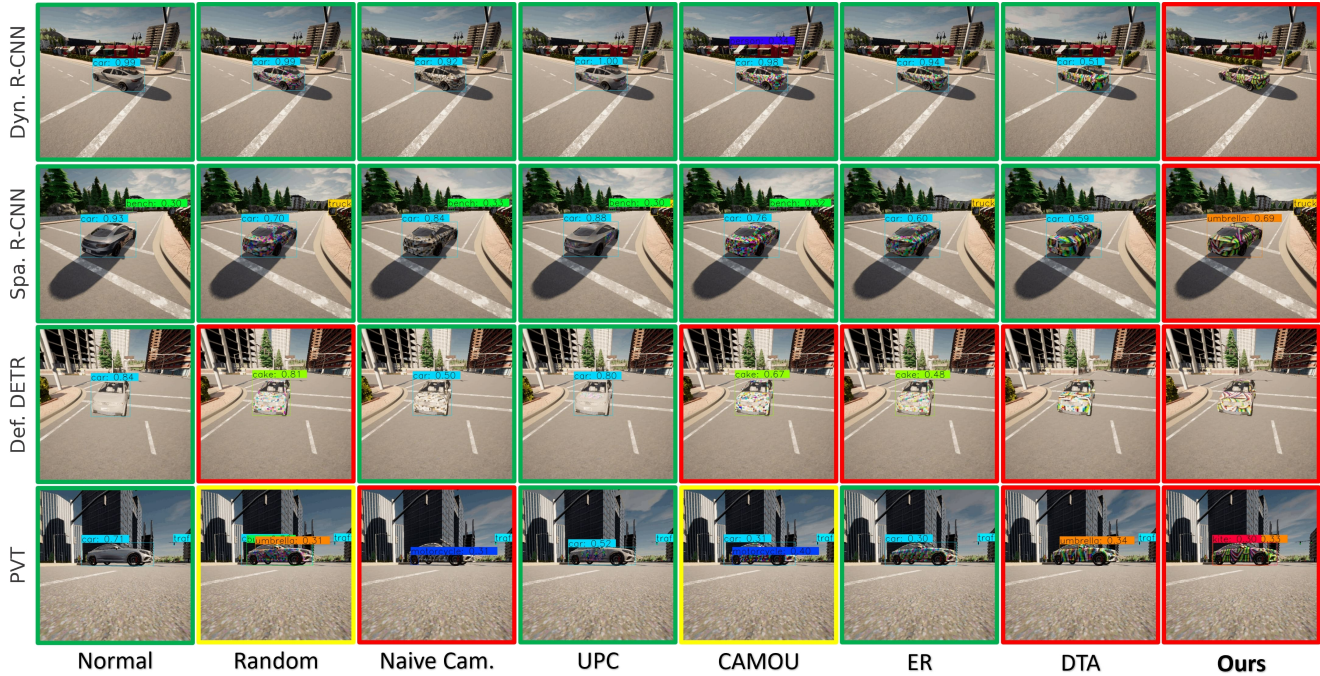


Figure 20: Sample predictions for each method on various models and cars. Green = correct; Yellow = partially correct; Red = misdetection. Zoom for detail.

F.2. Transferability to Different Class (Truck and Bus)

We perform evaluations to inspect whether the proposed adversarial camouflage can be transferred to other vehicle classes. We select a truck and a Volkswagen bus —which are available on the CARLA —as the target objects, and use the same textures and evaluated models from the previous evaluation. The detailed attack performance comparison for each method and evaluated model can be seen in Fig. 21, showing that our camouflage still performs best compared to others. Additionally, YOLOv7 sample prediction for each method and object can be seen in Fig. 22.

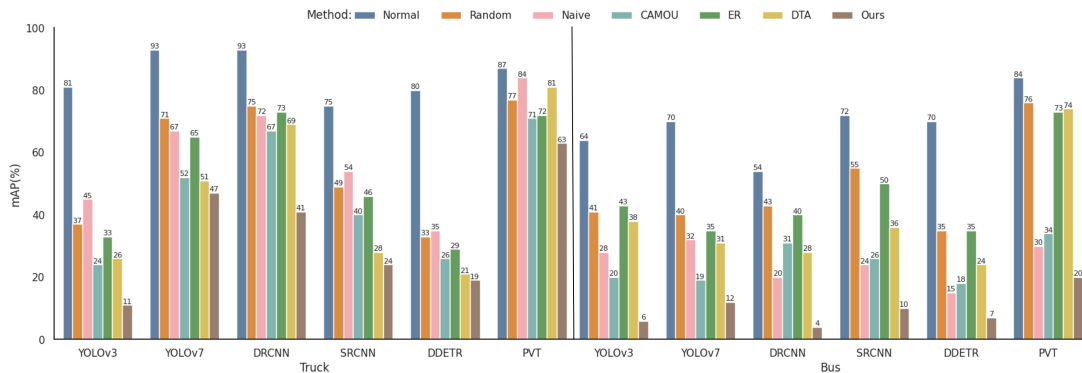


Figure 21: Transferability to different vehicle classes (truck and bus).

F.3. Transferability to Different Task (Segmentation Models)

We use segmentation models such as MaX-DeepLab-L [39] and Axial-DeepLab [40] to evaluate the transferability to different tasks. We evaluate the pixel accuracy of the car label to show how the adversarial camouflage can decrease the prediction of the target object. Fig. 23 shows that our method yields significantly higher attack performance compared to other methods, even for the segmentation models. Sample predictions can be seen in Fig. 24.

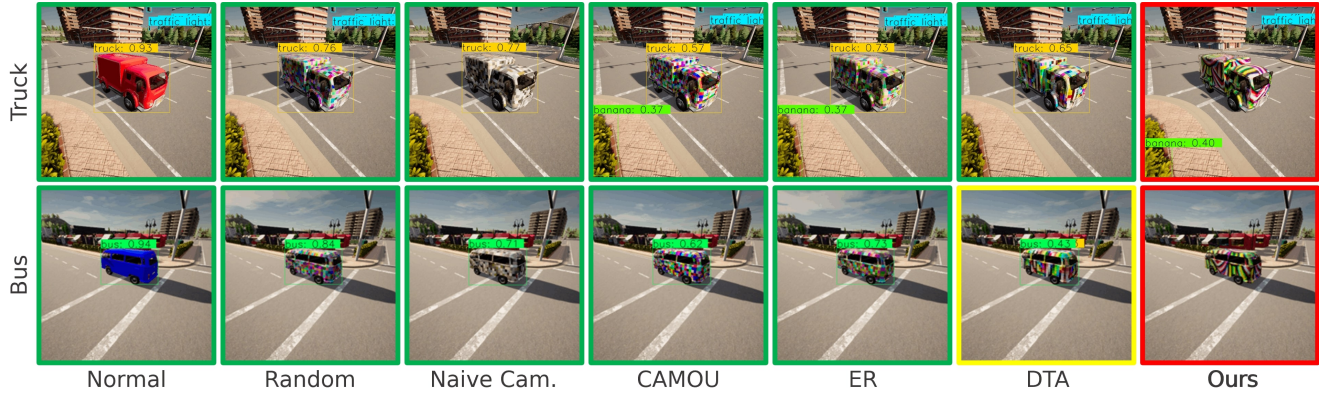
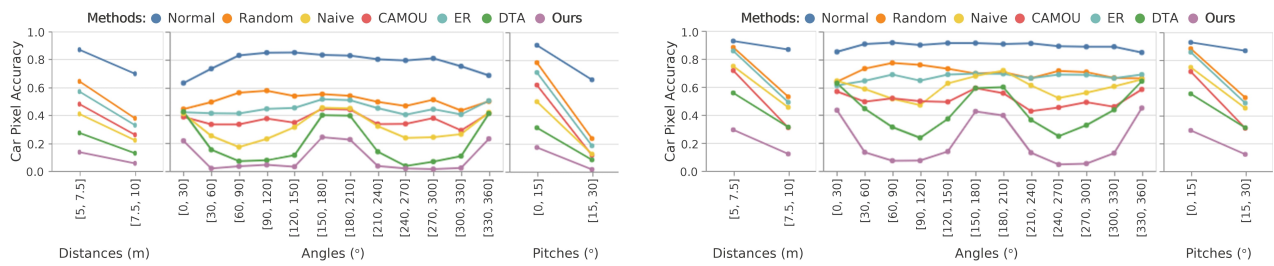
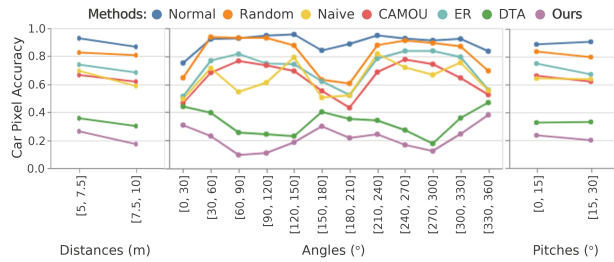


Figure 22: YOLOv7 sample predictions for truck and bus. Green = correct; Yellow = partially correct; Red = misdetection. Zoom for detail.



(a) Cityscape Pretrained MaX-DeepLab-L [39]

(b) Cityscape Pretrained Axial-DeepLab [40]



(c) COCO Pretrained MaX-DeepLab-L [39]

Figure 23: Transferability to segmentation models on different camera poses. Values are Pixel Accuracy of the target car.

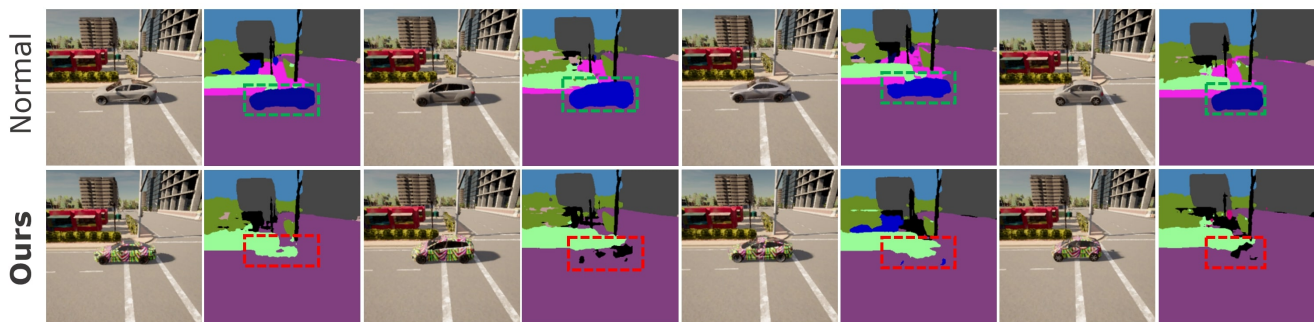


Figure 24: Sample predictions of normal and our camouflage car on Axial-DeepLab. The camouflage works universally on multiple cars.

F.4. Transferability to the Real World

We conduct a real-world experiment by fabricating two 1:10-scaled Tesla Model 3s with a 3D printer: one for a normal and another for our camouflaged car with the texture targeting YOLOv3. We select the adversarial camouflage with the best attack performance (i.e., the lowest AP of YOLOv3) to reliably measure the transferability to the real world when producing a camouflaged car. We place the car models in five real-world locations and capture car images for every 45-degree interval in angles ([0, 45], [45, 90], . . . , [315, 360] degrees) with three different distances ([5, 7.5], [7.5, 10], [10, 12.5] meters) and two different pitches ([0, 15], [15, 30] degrees) using iPhone 11 Pro Max. As a result, a total of 240 images (5 locations × 8 rotations × 3 distances × 2 pitches) are taken for each camera pose, and 240 images for each car model. In summary, a total of 480 images are used for evaluation.

We evaluate practical real-time object detectors widely used in the real world: MobileNetV2 [29], EfficientDet-D2 [33], YOLOX-L [14], and YOLOv7 [36]. From Fig. 25, our adversarial camouflaged car can significantly decrease AP@0.5 of all object detection models in the real world. Fig. 26 shows that the normal car model is well detected, whereas the camouflaged car model is not detected as a car at all under various camera poses.

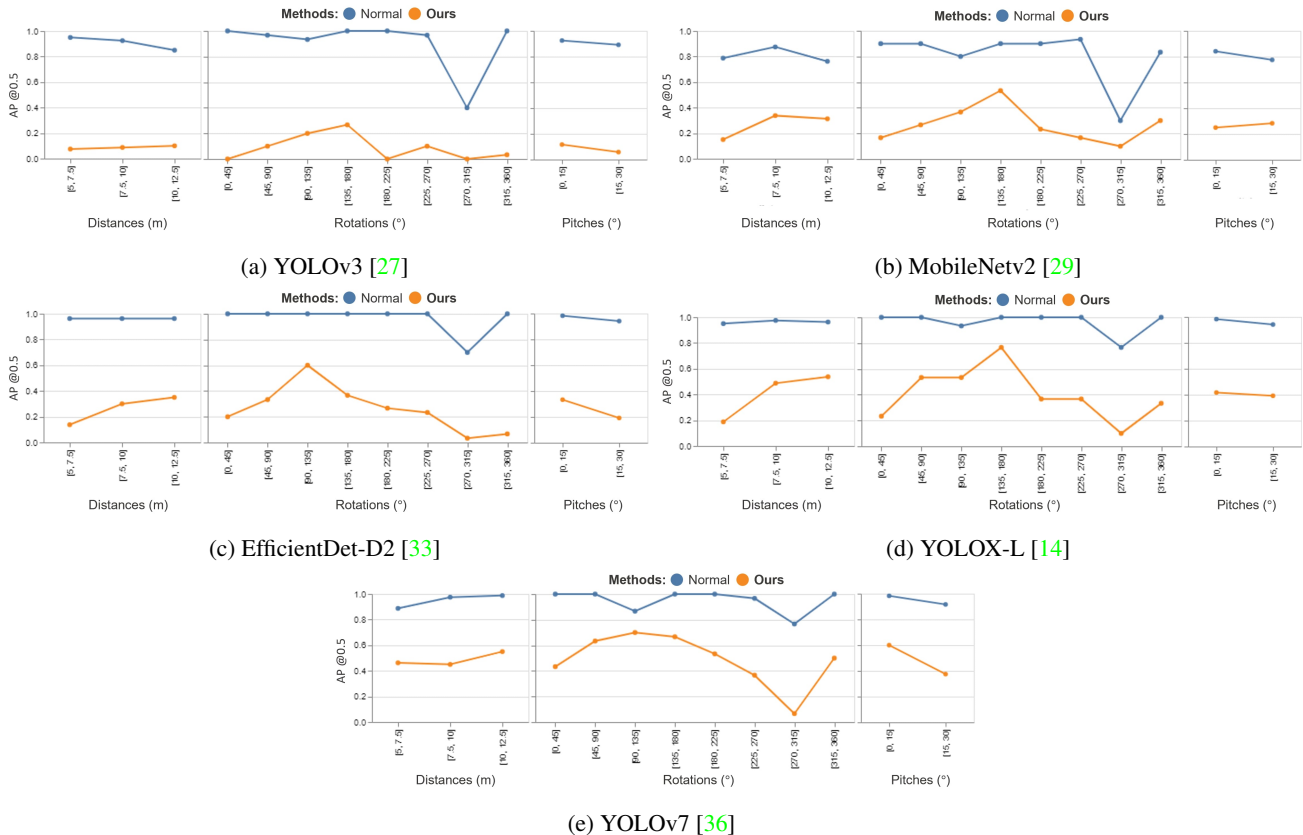


Figure 25: Transferability to real world on different camera poses. Values are Average Precision @0.5 of the target car.



(a) Normal car. Cars can be consistently detected with relatively high scores.



(b) Our camouflaged car. It can evade most of the detection with a high success rate, while background objects can still be detected correctly.

Figure 26: Sample predictions of our real-world evaluation using two scaled car models. We randomly sample 240 real-world images for a single car consisting of five locations, three distances, eight rotations, and two pitch angles as camera transformation sets. Zoom for detail.

G. Ablation Study

G.1. Effect of Different Losses With Respect to Performance

We perform a detailed analysis of our loss hyperparameters, including our smooth loss β and camouflage loss γ with respect to the attack performance in the white-box setting (targeting YOLOv3). We fix our stealth loss α as 1.0 and run a grid search for both β and γ with the value in the range of $[0.0, 0.25, 0.5, 0.75, 1.0]$. As shown in Fig 27, the smooth loss has a better correlation for increasing the attack performance than camouflage loss. Also, as mentioned by [24], extreme differences between adjacent pixels in the perturbation are unlikely to be accurately captured by cameras and may not be physically realizable; thus, the smooth loss becomes important in physical adversarial attacks, as verified in our experiment. On the other hand, utilizing our camouflage loss may result in a trade-off between attack performance and naturalness since it suppresses texture by using colors close to the extracted dominant background, limiting the use of other colors to enhance the attack. This can be seen from the AP@0.5 grouped by camouflage γ showing that $\gamma = 0$ has the lowest mean compared to others.

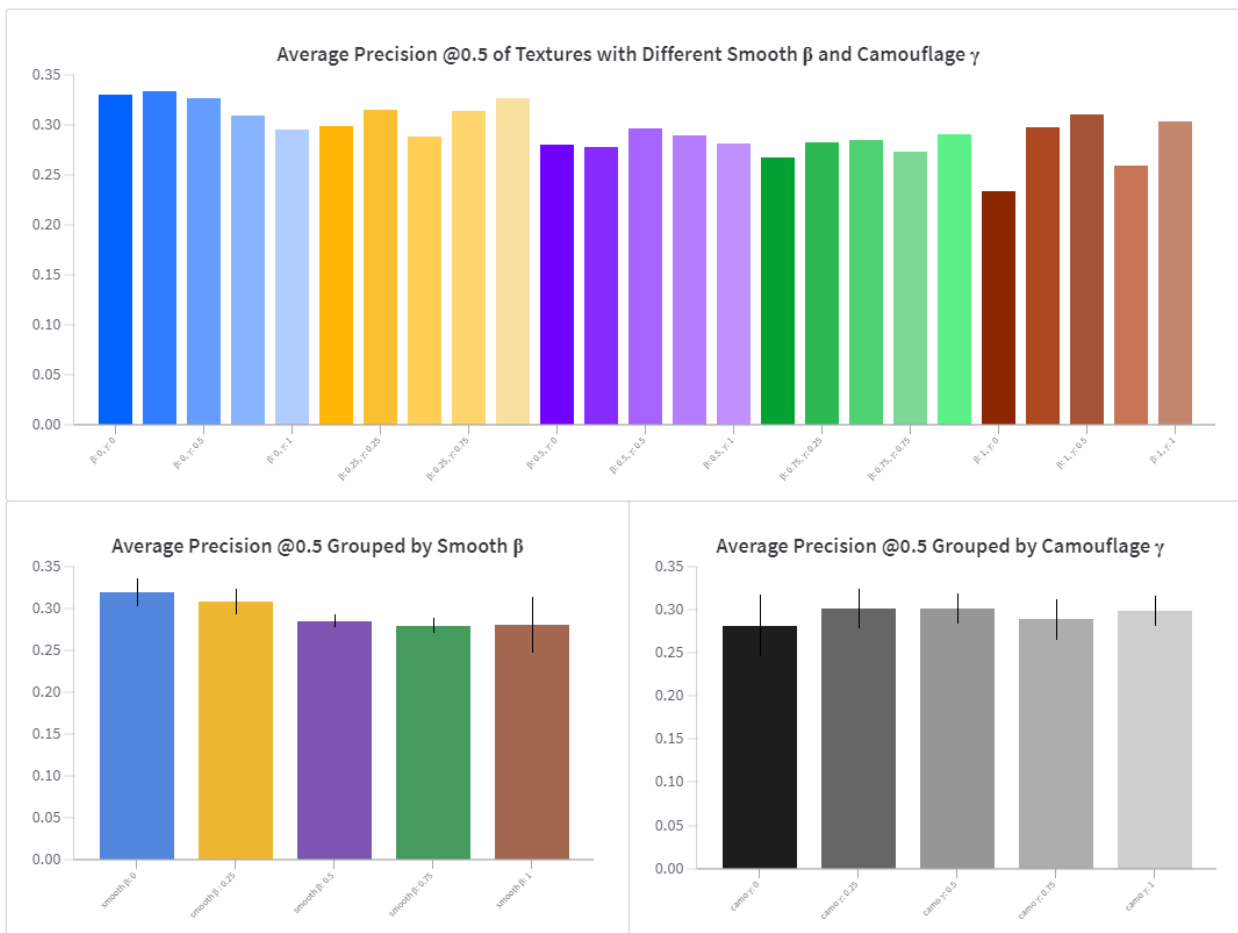


Figure 27: Performance graph for various smooth loss β and camouflage loss γ .

G.2. Effect of Different Losses with Respect to Naturalness

Here, we visualize the effect of different losses with respect to texture naturalness. As shown in Fig 28, we can see that both smooth and camouflage loss have a role in texture naturalness. We also observe that higher smooth β results in lower pixels variance, yielding a smooth texture, while higher camouflage γ results in softer color texture. Additionally, only utilizing the smooth loss may result in a bright and garish color texture, attracting more human attention, whereas only employing camouflage loss may result in a rough texture. Thus, utilizing both smooth and camouflage loss yields in a more natural result with a smoother and softer texture.

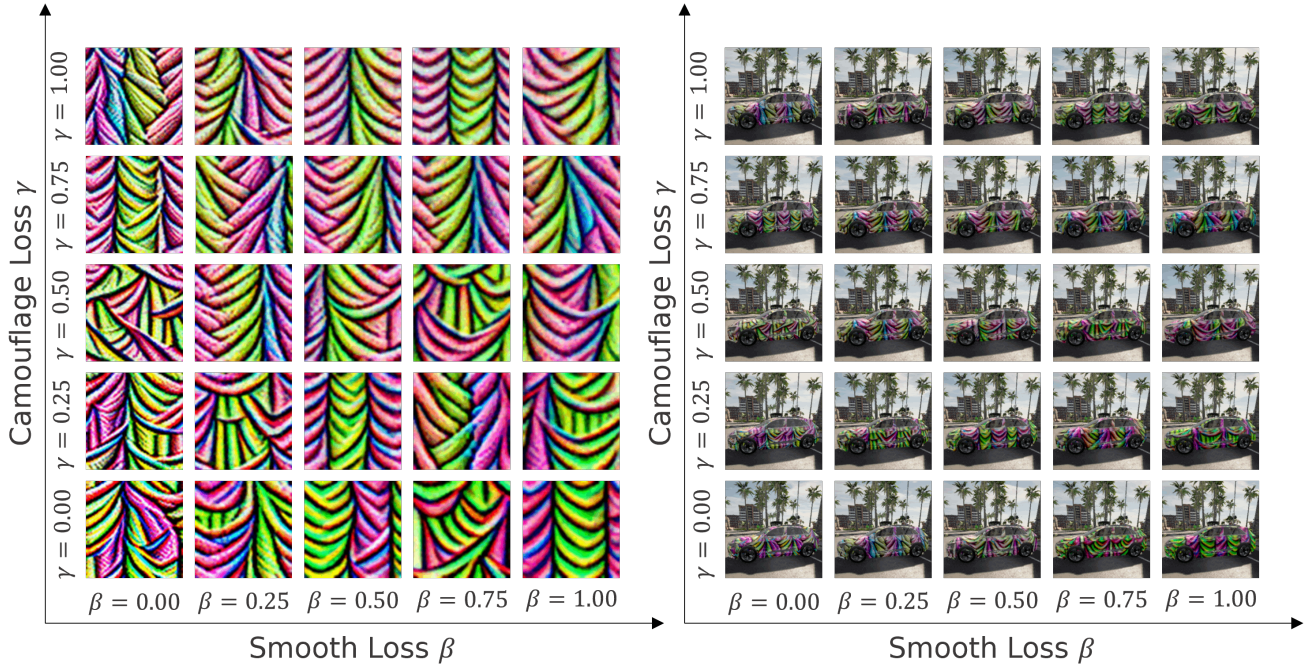


Figure 28: Our optimized adversarial camouflage texture with various smooth loss β and camouflage loss γ : base texture (left), after rendered in UE4 (right).

G.3. Effect of Different Target Models

We conduct experiments using a state-of-the-art (SOTA) model to assess how different target models affect attack performance. The results of our experiments are presented in Table 11, indicating that when targeting YOLOv7, a more robust model, we obtain a corresponding increase in the robustness of the texture.

Table 11: Universality evaluation on SOTA target model (YOLOv7)

Methods (Target)	Evaluated Model - Car AP@0.5					
	YOLOv3	YOLOv7	DRCN	SRCN	DDETR	PVT
Normal	85.98	92.54	83.20	82.55	83.83	88.59
Ours (YOLOv3)	22.55	41.55	30.38	42.00	14.69	51.54
Ours (YOLOv7)	33.13	20.98	15.33	17.98	10.11	32.43